EFFECT OF MODAL TRUNCATION ON DERIVATIVES OF CLOSED-LOOP DAMPING RATIOS IN STRUCTURAL CONTROL

by

Chris A. Sandridge

Dissertation submitted to the Faculty of the
Virginia Polytechnic Institute and State University
in partial fulfillment of the requirements for the degree of
Doctor of Philosophy
in
Aerospace Engineering

APPROVED:

Raphael T. Haftka, Chairman

Eric R. Johnson

Rakesh K. Kapania

Frederick H. Lutze, Jr.

Menahem Baruch

April, 1989

Blacksburg, Virginia

EFFECT OF MODAL TRUNCATION ON DERIVATIVES OF CLOSED-LOOP DAMPING RATIOS IN STRUCTURAL CONTROL

by

Chris A. Sandridge

Committee Chairman: Raphael T. Haftka

Aerospace and Ocean Engineering

(ABSTRACT)

It is well known that Fourier series of discontinuous functions converge slowly and that the derivatives of the series may not converge at all. Since modal expansion of structural response is a generalization of the Fourier series, slow convergence of modal expansion can be expected when the applied loads exhibit discontinuities in time or space. Thus, in a structure controlled by point actuators, slow convergence of derivatives of structural response with respect to system parameters can be expected. To demonstrate this, the sensitivity of the closed-loop response to structural changes is calculated for a multi-span beam with three control systems of increasing complexity that utilize point actuators. Reduced models based on the natural modes of the structure are formed and derivatives of the damping ratios of the closed-loop eigenvalues are calculated. As expected, the convergence of the derivatives of the damping ratios with increasing number of modes is slower than the convergence of the damping ratios themselves. The convergence is improved when distributed actuators replace the point actuators. When the control system is designed based on a reduced model, the damping ratios also converge slowly.

In transient response problems, it is known that complementing the vibration modes with a mode representing static response to the loads can greatly improve

convergence. Indeed, for the examples studied, when Ritz vectors corresponding to static responses due to unit loads at the actuators are added to the basis vectors, the convergence of the reduced-model derivatives is greatly enhanced. Also, when the control system is designed using a reduced model containing both vibration modes and Ritz vectors, its prediction of the full-model response is greatly improved.

Acknowledgements

I would like to thank my advisor Raphael T. Haftka for serving as my committee chairman. His dedication, insight, and humor have made the last four years most enjoyable. I would also like to thank the other members of my committee: Rakesh Kapania, Eric Johnson, Frederick Lutze, Menahem Baruch, and William Hallauer. They have all been helpful.

I appreciate the support of NASA Langley Research Center for the grant NAG-1-603, which supported this research. I would also like to thank the Interdisciplinary Research Office for allowing me to spend a year working with them. I especially wish to thank and for helping me tame the Cyber and Vax computers.

I would like to thank the Aerospace and Ocean Engineering Department for their financial support via a Pratt Fellowship and tuition waiver. I would also like to thank the secretaries, , , and , for their friendly help.

I will always have good memories about my fellow students in Femoyer Hall. They have become a second family to me and I will always remember to good times we had together.

Finally, I wish to thank my parents, my mother and my late father , for their encouragement to excel in academics and for giving me the opportunity to receive a college education. To my wife , I thank you most of all for your constant emotional support and love, and for putting up with the many weekends and evenings that I needed to work.

Table of Contents

List of Illustrations

List of Tables

Chapter 1

Introduction

Modern aerospace vehicles are highly complex and greatly coupled interdisciplinary systems. Traditional compartmental design procedures, in which each discipline (i.e. structures, aerodynamics, control) is designed separately, can produce final designs that are inefficient or infeasible. Therefore, interdisciplinary design procedures are necessary. For example, in hypersonic design, the coupling between structures, aerodynamics, control, and thermal considerations make interdisciplinary design necessary in order to produce a feasible design.[1] The interest in interdisciplinary design has grown so much in the past few years, that two conferences have been devoted to this area and the closely related subject of sensitivity analysis.[2-4]

Interdisciplinary design can also be beneficial for large space structures (LSS). Due to the high cost of transporting mass into space, space structures tend to be very flexible and have little inherent damping, thus active control systems are needed to damp out vibrations. Previously, the structure and the control system have been designed separately. First a structural engineer would design the structure to minimize the weight while meeting certain stress and geometric constraints.

Then a control engineer would design the control system to provide the necessary damping in the system. Recently, however, there has been interest in combined structure-control system design (see for example, Refs. 5 – 10).

Many different strategies were used for the combined design. Reference 5 shows that a synergistic effect exists between the control performance and structural parameters. It demonstrates that by adding concentrated masses at strategic locations on a structure, the control system effort can be reduced.

References 6–8 use variations on the idea of minimizing the mass of the structure while constraining closed-loop eigenvalues or damping ratios. References 9 and 10 included both control and structural design variables in the objective function; however, Reference 10 accomplished this indirectly by adding the mass of the control system actuators and power supply to the total mass of the structure. Then the mass of the control system was related to the control effort required to satisfy a specified response constraint.

One of the major problems in the design of control systems for LSS is how to accurately model the structure. The finite-element model of a structure can have thousands of degrees-of-freedom, which makes it impractical for use in control system design; therefore, some kind of reduced model must be used. In control system design, a reduced model based on a small number of vibration modes is typically used to model the structural dynamics. However, the errors associated with the reduced model can cause the control system to become unstable. For example, spillover instability is associated with the excitation of higher-order modes which are not included in the reduced model.[11] However, it is usually possible to overcome these instabilities by special techniques (e.g. Ref. 12), or by building in enough robustness into the control design.

The reduced models used for control design are usually based on the lowest natural vibration modes according to frequency. This procedure may neglect important higher frequency modes since for a LSS, the higher modes can still have very low frequencies and strong coupling with the lower modes. Modal cost analysis techniques were developed for choosing the best modes to include in the model.[13–17] Each mode is assigned a cost depending on characteristics of the mode, the type of control system, the type of analysis or design being performed, and the location of the sensors and actuators for the case of control design. Reference 15 also investigates the type of finite element to be used in the finite-element model of the structure. There are also model reduction schemes that are not based on vibration modes (e.g. Ref. 18).

In order to integrate the control and structural designs, the sensitivity of the control system to changes in the structure is needed. Errors associated with model reduction can be magnified by the process of differentiation. It has been shown that the convergence of the derivatives of the structural response with increasing number of modes can be much slower than the convergence of the response itself.[19] That is, more modes are required to accurately calculate the derivatives. The problem of slow modal convergence of derivatives can be expected to be more severe for large space structures which typically have a large number of closely spaced frequencies.

Modal expansion is a generalization of the Fourier series. It is well known that Fourier series of discontinuous functions converge slowly with respect to the number of series terms, and that the derivatives of the series may not converge at all. Accordingly, slow convergence of modal expansion can be expected when the applied loads exhibit discontinuities in time or space. This is demonstrated for the transient response of a string under a point load in Reference 20. In a controlled structure, where most of the damping is supplied by the control system,

convergence problems may be caused by point actuators. The purpose of this research is to demonstrate that such convergence problems can be encountered for the eigenvalues of the controlled system and to suggest a possible remedy.

In transient structural and thermal dynamics, methods have been developed which accelerate convergence when using mode superposition.[21–30] Refs. 28 and 29 use a pseudo-static load (mode-acceleration method) or Ritz vectors corresponding to static displacement to accelerate the convergence of a transient analysis. This dissertation will similarly show that Ritz vectors corresponding to static displacements due to unit loads at the actuators can improve convergence in both the control performance and its derivatives.

A simple multispan beam is investigated with three control systems of increasing complexity. The control systems are designed to produce similar damping in all three cases. The damping ratios and derivatives of the damping ratios with respect to structural parameters are calculated with the full finite-element model and compared with similar calculations using reduced models.

It will be shown that reduced models based only on vibration modes are very poor for calculating derivatives of the damping ratios with respect to structural parameters when point actuators are used. However, it will also be shown that if Ritz vectors corresponding to static displacements due to unit loads at the actuator locations are added to the reduced basis, the accuracy of the derivatives is greatly improved.

Chapter 2 describes a study involving a direct-rate feedback control system with colocated velocity sensors and force actuators. This is a good example to start with because it is easy to analyze and is guaranteed to be stable. The damping ratios and their derivatives with respect to both structural and control parameters are studied. Reduced models based on finite-element models of varying meshes

and an exact continuum model are investigated. Distributed control and very low damping control are also investigated. Ritz vectors added to the reduced models are shown to improve the convergence of both the damping ratios and their derivatives.

Chapter 3 discusses a more advanced control system consisting of an optimal Linear Quadratic Regulator (LQR) and a simple modal filter. The convergence of damping ratios and their derivatives is again investigated so as to verify that the same conclusions reached in Chapter 2 apply to an optimal control system.

In Chapter 4, the more realistic Linear Quadratic Gaussian (LQG) control system is investigated. This consists of a LQR described in Chapter 3 coupled with a Kalman filter for state reconstruction. Analysis of this system is more difficult due to the observer poles in the closed-loop system. Also, the addition of Ritz vectors to this analysis is not as straight forward as in the previous analyses. Also, the effect of Ritz vectors in the *design* of the control system is investigated. It is well known that when a control system is designed using a reduced model, the design does not accurately predict the actual control on the structure. It is shown that Ritz vectors included in the reduced model improve the accuracy of the control design.

Finally, Chapter 5 summarizes the results of the previous chapters, forms some conclusions, and proposes areas for future research.

Most of the work reported in this dissertation can be found in more widely available form via References 31 and 32.

It should be noted that reference 33 describes another possible solution to the slow modal convergence shown in this dissertation. It utilizes a "ficticious mass" technique of component mode synthesis for generating an improved set of natural vibration modes. With the improved set, the reduced-model damping ratios and derivatives are shown to be more accurate than reduced-model values calculated using the natural vibration modes of the original structure.

Chapter 2

Rate-Feedback Control

In this chapter, a simply-supported, multispan beam controlled by a direct-rate feedback control system with colocated velocity sensors and force actuators is investigated. This type of control system can be thought of as an electric dashpot (i.e. the control force is proportional to the velocity at the controller), and since the forces always act opposite to the sensed velocities, the control system is always stable; i.e. there is no spillover.

In the introduction, it was stated that it is *well known* that Fourier series of discontinuous functions converge slowly and that the derivatives of the series may not converge at all. For completeness, this chapter starts by demonstrating this fact.

2.1 Convergence of Fourier Series and Derivative of a Step Function

Consider part of a periodic step function

$$f(x) = \begin{cases} 0 & -l \leq x < 0 \\ p & 0 \leq x < l \end{cases} \tag{2.1}$$

The Fourier series for the function is

$$f(x) = \frac{p}{2} + \frac{2p}{\pi} \sum_{m=1}^{\infty} \left(\frac{1}{2m-1} \right) \sin \left[\frac{(2m-1)\pi x}{l} \right] \tag{2.2}$$

The derivative with respect to the length of the interval l is

$$\frac{\partial f}{\partial l} = -\frac{2px}{l^2} \sum_{m=1}^{\infty} \cos \left[\frac{(2m-1)\pi x}{l} \right] \tag{2.3}$$

The derivative with respect to l was chosen since l changes the basis functions of the series much like a change in a structure would change the mode shapes in a modal analysis. Figure 2.1 shows the convergence of the series and its derivative for $p = .75$ at $x = l/10$, [The exact values are $f(l/10) = .75$ and $\frac{\partial f}{\partial l}(l/10) = 0$]. The figure shows that even though the function converges fairly quickly, the derivative never converges. This demonstrates that sines and cosines are not good basis functions for describing the derivative of a step function. Similarly, it will be shown that mode shapes are not a good set of basis functions for calculating the derivative of closed-loop eigenvalues when point actuators are used.

2.2 Eigenvalue Derivative Calculation

2.2.1 *Finite-Element Formulation*

The equations of motion for an n degree of freedom structure with direct rate feedback control produced by velocity sensors and force actuators are

$$M\ddot{\mathbf{q}} + D\dot{\mathbf{q}} + K\mathbf{q} = 0 \tag{2.4}$$

where M, D, and K are the mass, damping, and stiffness matrices and $\mathbf{q}$ is the structural response vector. The inherent damping of the structure is neglected in this chapter so that for colocated velocity sensors and force actuator pairs, the

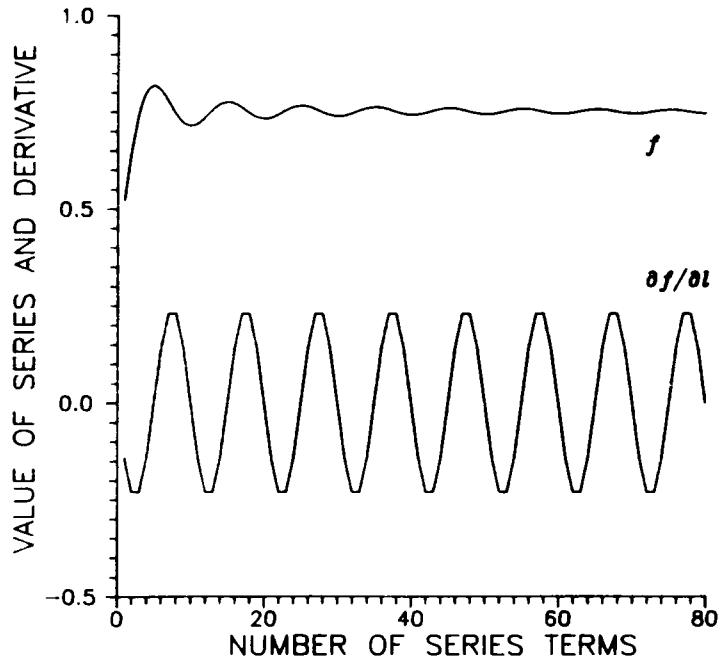

Figure 2.1: Convergence of Fourier Series of a Step Function and its Derivative

damping matrix (D) has nonzero entries (d_i) on the diagonal corresponding to the location of the sensor-actuator pair. The value of d_i depends on the magnitude of the control gain. Assuming a solution of the form

$$\mathbf{q}(t) = \mathbf{q_k} e^{\lambda_k t} \tag{2.5}$$

the associated eigenvalue problem is

$$\left[\lambda_k^2 M + \lambda_k D + K\right] \mathbf{q_k} = 0 \tag{2.6}$$

The solution of Eq. (2.6) yields $2n$ real and complex eigenvalues

$$\lambda_k = \sigma_k + i\omega_k \qquad\qquad k = 1, \ldots, 2n \tag{2.7}$$

where σ_k and ω_k are the real and imaginary parts of the eigenvalues. For the lightly damped systems discussed in this dissertation, the eigenvalues are complex conjugate pairs.

The damping ratio (ζ_k) is defined as

$$\zeta_k = \frac{-\sigma_k}{\sqrt{\sigma_k^2 + \omega_k^2}} \tag{2.8}$$

The damping ratio is a measure of the effectiveness of the control for a particular mode, and it is used here to represent the control system performance.

To find the derivative of the damping ratio (ζ_k) with respect to a structural parameter, it is necessary to calculate the derivative of the eigenvalue. Differentiating Eq. (2.6) with respect to a structural parameter, it is seen that

$$\left[\lambda_k^2 M + \lambda_k D + K\right]\mathbf{q_k}' + \left[2\lambda_k\lambda_k' M + \lambda_k^2 M' + \lambda_k' D + \lambda_k D' + K'\right]\mathbf{q_k} = 0 \tag{2.9}$$

where the primes denote derivatives with respect to the structural parameter. Equation (2.9) is pre-multiplied by $\mathbf{q_k}^T$ and then simplified to get

$$\lambda_k' = -\frac{\lambda_k^2 \mathbf{q_k}^T M' \mathbf{q_k} + \lambda_k \mathbf{q_k}^T D' \mathbf{q_k} + \mathbf{q_k}^T K' \mathbf{q_k}}{2\lambda_k \mathbf{q_k}^T M \mathbf{q_k} + \mathbf{q_k}^T D \mathbf{q_k}} \tag{2.10}$$

Equation (2.10) can be expressed as

$$\lambda_k' = \sigma_k' \pm i\omega_k' \tag{2.11}$$

The derivative of the damping ratio can now be calculated by differentiating Eq. (2.8) to get

$$\zeta_k' = \frac{\omega_k(\sigma_k\omega_k' - \omega_k\sigma_k')}{(\sigma_k^2 + \omega_k^2)^{3/2}} \tag{2.12}$$

To calculate the derivative of the damping ratio with the full finite-element model, first solve Eq. (2.6) for the eigenvalues and eigenvectors. Then calculate the derivative of the mass, stiffness, and damping matrices either by finite differences or analytically. Use Eq. (2.10) to calculate the derivative of the eigenvalue and finally, calculate the derivative of the damping ratio from Eq. (2.12). The derivative obtained by this process is denoted the "full-finite-element" derivative.

2.2.2 *Reduced-Model Formulation*

Assume the displacement can be approximated as a linear combination of N modes

$$\mathbf{q} = \sum_{i=1}^{N} \phi_i v_i \qquad N < n \tag{2.13}$$

where $\phi_\mathbf{i}$ is the i^{th} natural mode shape and v_i is the modal amplitude. The reduced eigenvalue problem corresponding to the modal coordinates is

$$\left[\lambda_k^2 \hat{M} + \lambda_k \hat{D} + \hat{K}\right] \mathbf{v_k} = 0 \tag{2.14}$$

where $\mathbf{v_k}$ is the k^{th} reduced-model eigenvector and

$$\hat{M} = \Phi^T M \Phi \qquad \hat{D} = \Phi^T D \Phi \qquad \hat{K} = \Phi^T K \Phi \tag{2.15}$$

where Φ is a matrix with columns corresponding to the N modes used in the reduced model. When natural vibration modes are used, $\hat{M}$ and $\hat{K}$ are diagonal matrices, but for point actuators, $\hat{D}$, in general, is not diagonal.

There are several ways to calculate the derivatives of the damping ratios obtained from the reduced model. The first is to approximate $\mathbf{q_k}$ in terms of $\mathbf{v_k}$ using Eq. (2.13) and then use Eqs. (2.10) and (2.12) as before. A second approach is to proceed as in equations (2.10–2.12), replacing M, D, K, and $\mathbf{q_k}$ with $\hat{M}, \hat{D}, \hat{K}$, and $\mathbf{v_k}$ respectively. The derivatives of $\hat{M}, \hat{D}$, and $\hat{K}$ can be obtained in terms of the derivatives of M, D, K and Φ. For instance, $\hat{M}'$ is given as

$$\hat{M}' = \left[\Phi^T M \Phi\right]' = \Phi'^T M \Phi + \Phi^T M' \Phi + \Phi^T M \Phi' \tag{2.16}$$

If the modes used in Eq. (2.13) are fixed as the structure changes, the first and third terms in Eq. (2.16) are zero, which gives the same approximation as with the first approach above. This approximation is denoted here the "fixed-mode" derivative.

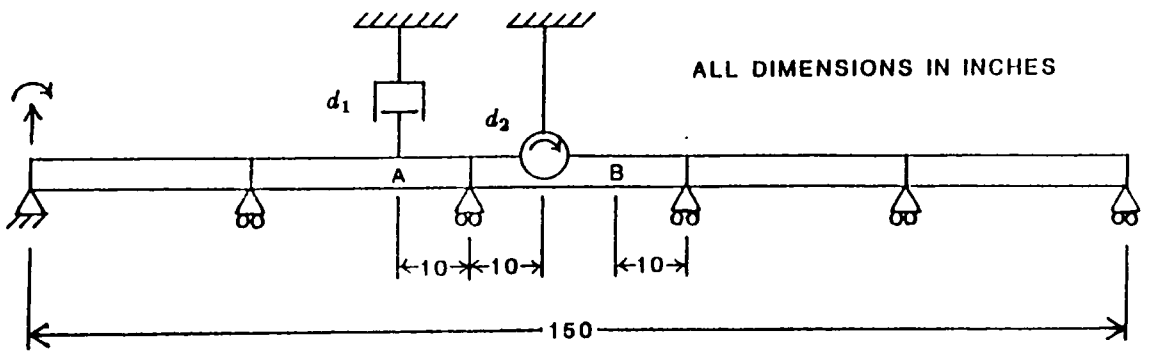

$A = 0.125$ in^2 $\quad \rho = 0.28$ lb/in^3
$E = (10)^6$ lb/in^2 $\quad I = 4.0 \times (10)^{-5}$ in^4

Figure 2.2: Multispan Beam Geometry

If the modes depend on the structure (as is the case with natural vibration modes), Eq. (2.16) requires the derivatives of the modes. Since this reduced-model derivative reflects the updating of the modes, it will be called the "updated-mode" derivative.

In the present work, the natural vibration modes of the structure are used to reduce the model. To avoid calculating derivatives of the updated modes in Eq. (2.16), ς_k' is calculated by finite differences. That is, the design variable is perturbed, new modes are calculated, a new reduced model is formed, and ς_k is recalculated.

2.3 Multispan Beam Example

To simulate a flexible space structure, a multispan, flexible beam (Fig. 2.2) was chosen because its frequencies are closely spaced. A closed-form, continuum solution (Ref. 34 and Appendix) is available for mode shapes and frequencies. However, since the formulation involves hyperbolic sine and cosine functions, quadruple numerical precision (128-bit floating-point precision) was needed to calculate the higher modes, and even then, only 60 modes could be calculated accurately.

The five-span beam was also modeled with beam finite elements using Engineering Analysis Language (EAL), a general purpose, finite-element and structural-analysis program.[35] EAL is composed of processors that perform calculations such as model formulation, stress analysis, and dynamic response. It is possible to add user-written processors which have access to the program data base. Most of the derivative calculations in this chapter were performed using EAL processors.

Several finite-element models of the beam were analyzed ranging from three elements per span (15 elements total) to twelve elements per span (60 elements total). Table 2.1 shows the first ten natural frequencies obtained from the continuum solution and from the three finite-element solutions.

Table 2.1 : Natural Frequencies(Hz) of Multispan Beam

	Continuum	Finite Element Models		
Mode	Model	15-Element	30-Element	60-Element
1	1.159223	1.160160	1.159281	1.159227
2	1.286099	1.287377	1.286179	1.286104
3	1.608256	1.610749	1.608414	1.608264
4	2.025720	2.030678	2.026035	2.025737
5	2.432052	2.440590	2.432600	2.432082
6	4.636892	4.691668	4.640615	4.637102
7	4.901461	4.965402	4.905860	4.901711
8	5.508898	5.596371	5.515144	5.509262
9	6.239599	6.357656	6.248659	6.240135
10	6.922233	7.063390	6.934594	6.922976

Two massless controllers were placed on the beam as shown in Figure 2.2; the first is a displacement-rate controller on the second span, and the second is a rotation-rate controller on the middle span. The controllers, which consist of a force (moment) actuator colocated with a velocity sensor, act as viscous dampers with damping constants d_1 and d_2, and they were designed to produce damping

ratios between one and ten percent for the first ten modes. Table 2.2 shows the damping ratios of the first ten modes for the three finite-element models, with $d_1 = 0.008$ lb-s/in and $d_2 = 1.2$ lb-in-s. From Tables 2.1 and 2.2 it is clear that even the coarsest model is quite accurate for the first six frequencies and damping ratios.

Table 2.2 : Damping Ratios of First Ten Modes

Mode	15-Element	30-Element	60-Element
1	.0907109	.0904736	.0904462
2	.0255612	.0255043	.0254988
3	.0778104	.0774696	.0774506
4	.0574582	.0571145	.0570915
5	.0955770	.0947231	.0946659
6	.0145501	.0143603	.0143460
7	.0312876	.0300424	.0299601
8	.0145351	.0142391	.0142142
9	.0392655	.0376863	.0375407
10	.0195291	.0188517	.0187872

The structural design variable used in the sensitivity analysis is the addition of a concentrated mass at points A or B on the beam (see Fig. 2.2). To begin, the addition of a mass at point A is studied. First, the damping ratios (ς_k) and the derivatives of the damping ratios with respect to a concentrated mass were calculated analytically using the full finite-element model. Then the vibration modes were calculated for the finite-element model, and reduced-model derivatives of the damping ratios were computed for increasing number of modes (up to a number of modes equal to the number of unrestrained degrees of freedom in the finite-element model). The fixed-mode derivatives were calculated analytically. The updated-mode derivatives were calculated by central finite differences as

$$\varsigma_k' \cong \frac{\varsigma_k(\Delta m) - \varsigma_k(-\Delta m)}{2\Delta m} \tag{2.17}$$

Figure 2.3 shows the value of ζ_1' as a function of the step size (Δm) using 15 modes and the 15-element model. For small values of Δm, accuracy is poor due to roundoff errors, while for large values of Δm, the truncation error is excessive. A step size of 5×10^{-7} lb-s^2/in was selected.

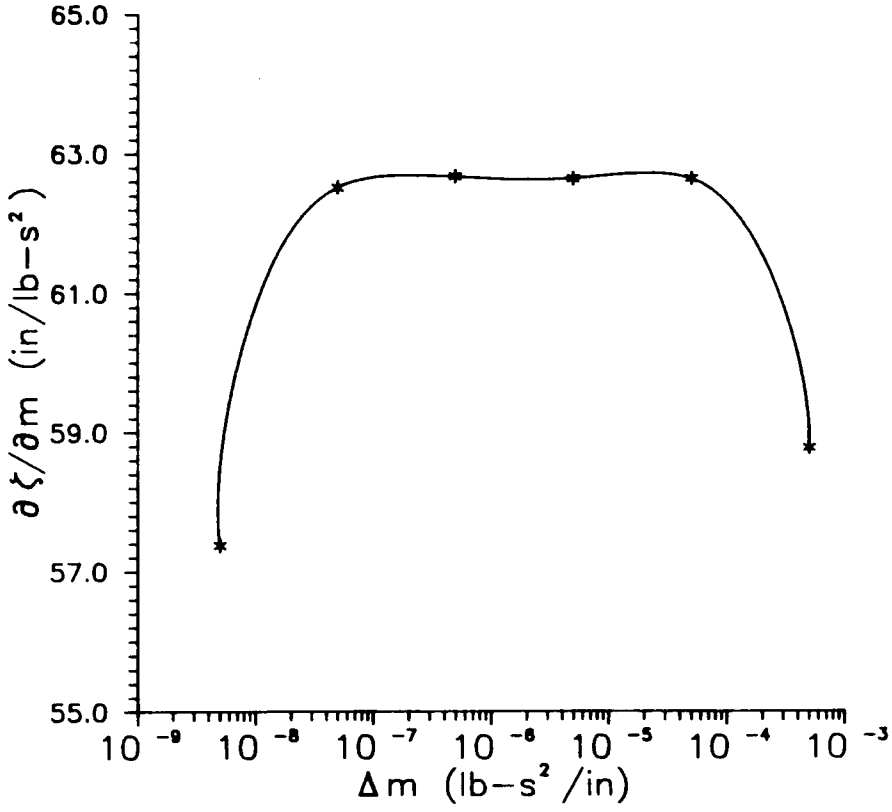

Figure 2.3: Derivative of First Damping Ratio Vs. Finite-Difference Step Size

2.4 Error in Derivative of Damping Ratio

2.4.1 *Coarse Finite-Element Model*

The first set of results were obtained for the 15-element model, which has 26 unrestrained degrees of freedom. The first six damping ratios for this model have

errors of less than 1.5% (with respect to the 60-element model), while the seventh damping ratio has more than 4% error. Therefore, derivatives of the first six damping ratios with respect to the added mass were calculated using the finite-element model without any modal approximation (see Table 2.3).

Table 2.3 : Derivatives of First Six Damping Ratios With Respect to Added Mass at Two Locations (refer to Fig. 2.2)

	Derivative ($in/lb\text{-}s^2$)	
Mode	Point A	Point B
1	65.72374	20.47085
2	-19.62912	7.540893
3	-34.53779	-34.16656
4	3.3944869	22.11590
5	-31.18742	6.653129
6	55.11845	36.93203

Next, damping ratios and their derivatives based on reduced models with up to 24 modes were calculated. Errors in the damping ratios and their derivatives were calculated with respect to the full-finite-element results. Figures 2.4, 2.5, and 2.6 show the absolute value of the relative errors in the second, fourth, and sixth damping ratios, respectively, and their respective derivatives versus the number of modes in the reduced model. The solid line represents the error in the damping ratio and dashed lines represent the errors in the updated-mode and the fixed-mode derivatives. Clearly, and not surprisingly, the errors in the derivatives are much larger than the errors in the corresponding damping ratios.

The fixed-mode and updated-mode derivatives were of comparable accuracy. The agreement between the two types of derivatives indicates that the errors associated with the finite-difference calculation of the updated-mode derivatives are small.

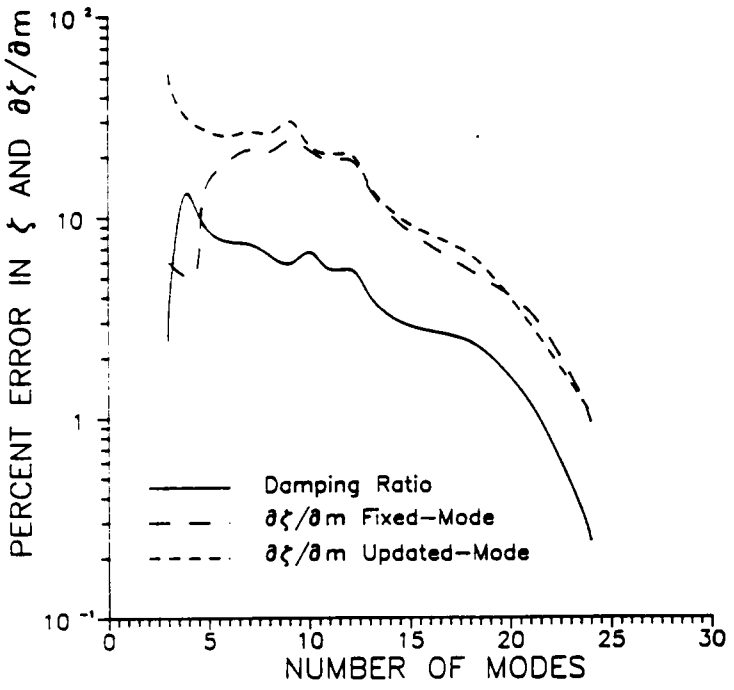

Figure 2.4: Convergence of Mode 2 Damping Ratio and its Derivative

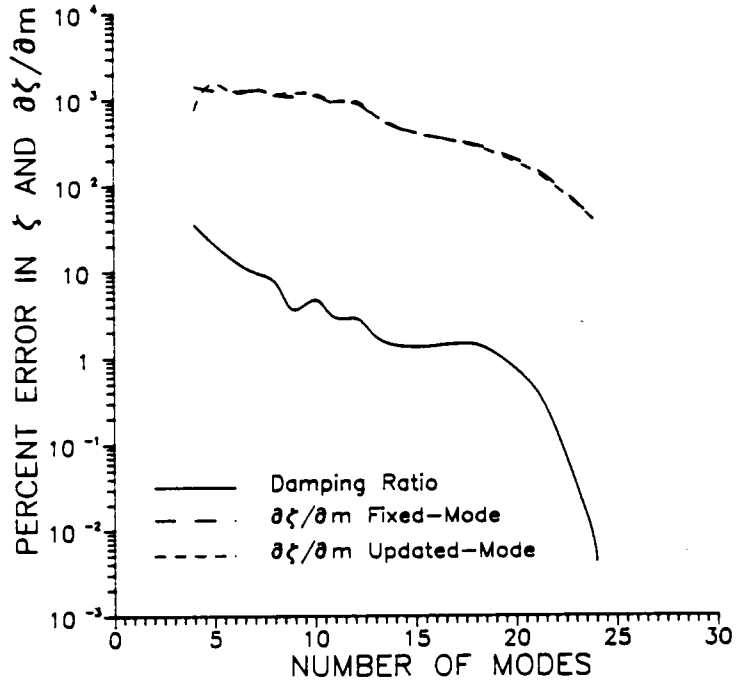

Figure 2.5: Convergence of Mode 4 Damping Ratio and its Derivative

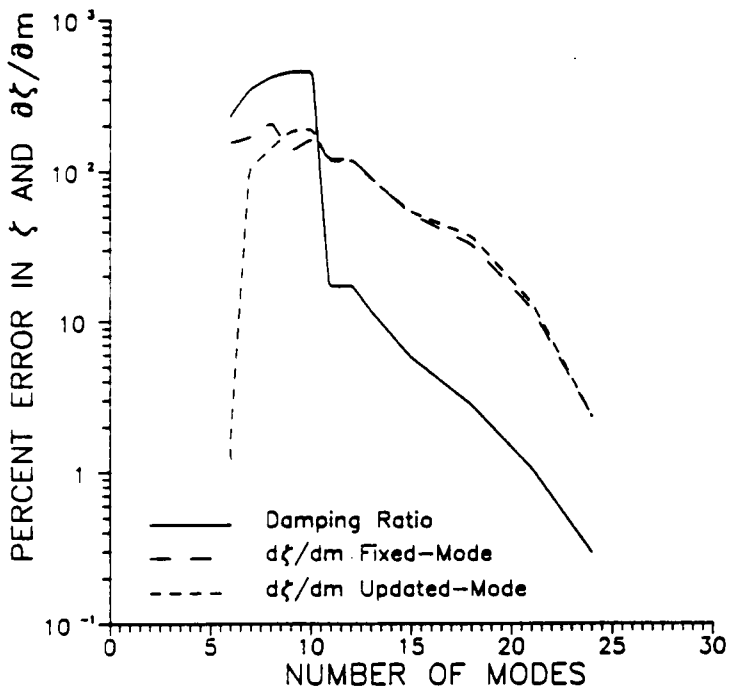

Figure 2.6: Convergence of Mode 6 Damping Ratio and its Derivative

The results of damping ratios and their corresponding derivatives for other modes are similar to those presented in that errors in the derivatives are about an order of magnitude larger than the errors in the damping ratios. The comparison of the fixed-mode and the updated-mode derivatives indicates that in the zone where the errors are acceptable, there is no substantial difference between the two methods; thus the cheaper, fixed-mode method is preferred.

The convergence of the reduced-model derivatives is also a function of the damping in the system. For lower damping, the coupling between the modes decrease and the convergence rate is accelerated. For example, Figure 2.7 shows the convergence of the fourth mode damping ratio and its derivative for gains (d_1 and d_2) that are reduced by one half. This figure shows that for one-half decrease in the damping in the system, the errors in the derivative are reduced by an order of magnitude (compare with Fig. 2.5).

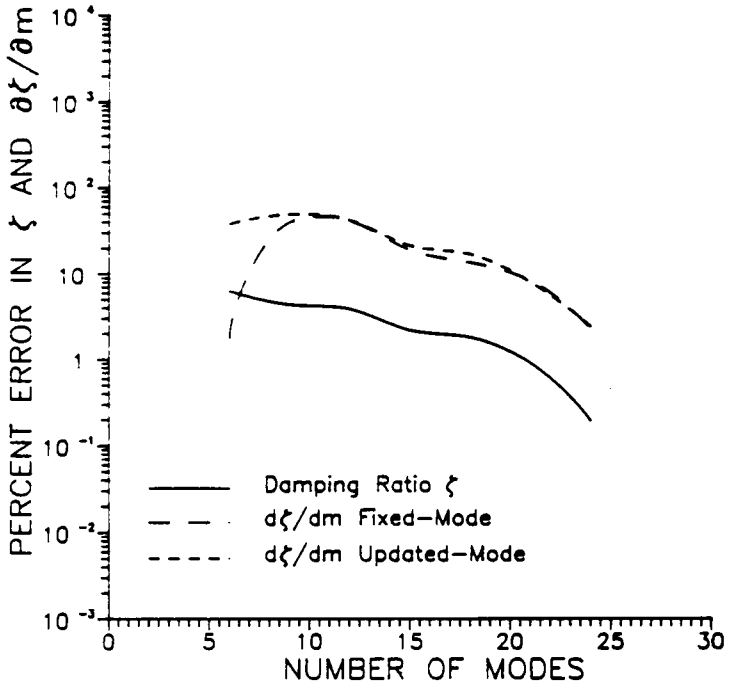

Figure 2.7: Convergence of Mode 4 Damping Ratio and its Derivative with Reduced Damping

As in the Fourier example (Fig. 2.1), it has been shown that while the convergence of the damping ratios is good, the convergence of the derivatives of the damping ratios can be poor. However, the modal convergence is misleading when the number of modes approaches the number of degrees of freedom of the finite-element model. When the number of modes is equal to the number of degrees of freedom, the modal and finite-element analyses are identical. Therefore, the accelerated convergence seen in Figures 2.4–2.6 when the number of modes exceeds 20 may be a consequence of the use of finite-element modes instead of exact modes. To check on this possibility, more refined models were investigated.

2.4.2 *Refined Finite-Element Models*

To further explore the slow convergence of the fourth-mode derivative, finite-element models with finer meshes, including 6, 9, and 12 beam elements per span

(30, 45, and 60 total elements, respectively) were formed. The reduced-model, updated-mode derivatives were calculated, and the errors were referenced to an "exact" derivative value calculated by extrapolating the derivative calculated using the two finest meshes as follows.

Reference 36 shows that the error in the finite-element eigenvalues decreases asymptotically with the fourth power of the number of cubic beam elements used in the finite-element model. This can be applied to the derivative of the eigenvalue (thus the derivative of the damping ratio) to give us the relation

$$f_n = f_0 - \alpha n^{-4} \tag{2.18}$$

where f_n is the finite-element derivative obtained with n elements, f_0 is the exact value of the derivative, and α is a constant. The values f_0 and α were calculated for the fourth-mode derivative using the results of the 45- and 60-element models. The value of f_0 obtained (3.56527 in/lb-s^2) was used as the "exact" value of the derivative.

To complete the analogy with the Fourier example, the fourth damping-ratio derivative was also calculated using gradually increasing, reduced-order models based on continuum modes (see Appendix). As in a Fourier series, the continuum formulation gives us an infinite number of modes to work with. Also, the continuum modes are exact, as opposed to the approximate modes produced by the finite-element formulations. Again, the errors were calculated with respect to the "exact" value calculated above.

Three types of models are now available. Two use vibration modes, one with finite-element modes and one with continuum modes, and the third is the full-finite-element model. The order of the model for the first two types is equal to

the number of modes while for the third it is equal to the number of finite-element degrees of freedom.

The errors in the derivative of the fourth damping ratio for the three types of models are given in Figure 2.8 as a function of the order of the model. The top solid line is the error in the derivative calculated using the continuum modes (see Appendix). The dashed lines are the errors in the derivative for the four finite-element models using updated modes (and finite differences), and the bottom solid line is the error in the four, full-finite-element derivatives, using Eqs. (2.10–2.12).

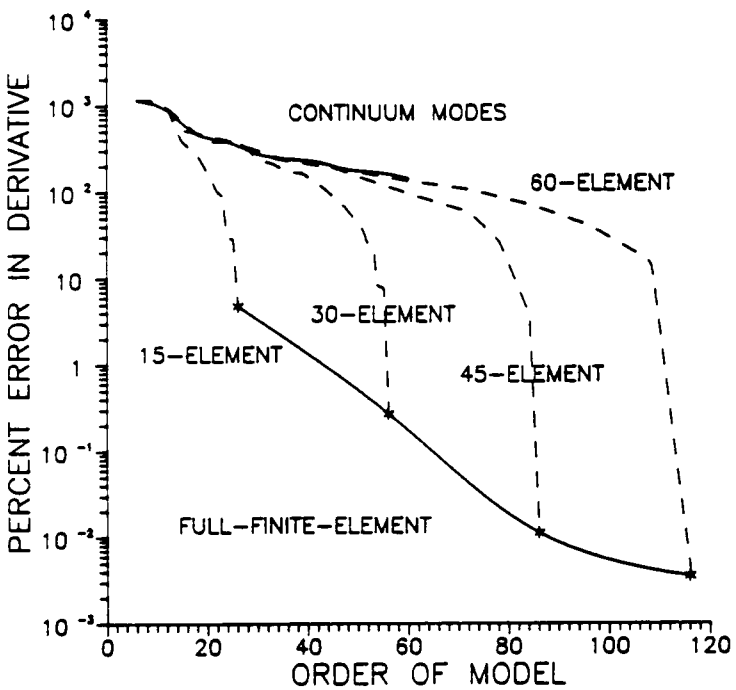

Figure 2.8: Convergence of Mode 4 Derivative — Reduced Models and Finite-Element Models

From Figure 2.8 it is clear that the convergence of the continuum, reduced-model derivative is much slower than the finite-element derivative. For the same order, the finite-element derivative is two to four orders of magnitude more accurate. For example, with 26 degrees of freedom, the coarsest finite-element model

has an error of about 5%, whereas 26 continuum modes result in an error of about 350%. Clearly, for this problem, the use of vibration modes to reduce the model is counterproductive.

Following the convergence of any of the finite-element, reduced-model cases, it is seen that for the low-order models, the convergence follows that of the continuum case. This is expected since the lower modes of a finite-element formulation are quite accurate. But as the higher, *less* accurate modes are added, the rate of convergence *increases*. This is not because the less accurate modes are better at calculating the derivative; it is because, when all of the modes of the finite-element model are included, the result must be the same as for the full-finite-element model. Thus the reduced-model, finite-element derivatives eventually converge to the full-finite-element value. This produces the paradoxical result that for a fixed number of modes, the accuracy of the derivative *deteriorates* as the finite-element model is refined. For example, with the coarsest model, 26 modes give the same derivative as the full-finite-element calculation, i.e., an error of 5%. When 26 modes are used with the 30-element model, the derivative is very close to the continuum results, thus the error increases to about 350%.

2.4.3 *A Different Derivative*

So far, only the derivative with respect to an added mass has been examined. The reason for this is that it is easy to calculate the analytical derivative of the mass matrix. However, it is necessary to show that poor convergence occurs for derivatives with respect to other parameters. To demonstrate this, the derivatives of the damping ratios with respect to the cross-sectional width (b) of the beam are calculated using the updated-model, finite-element technique.

The same convergence study as described earlier is performed on the 26-mode model. Figure 2.9 shows the convergence of the mode 2 damping ratio and derivative with respect to the width of the beam. This shows that the derivative does not converge to within 10% until 23 out of 26 modes have been included in the reduced model. This example is sufficient to prove that poor convergence can occur for derivatives with respect to other structural parameters.

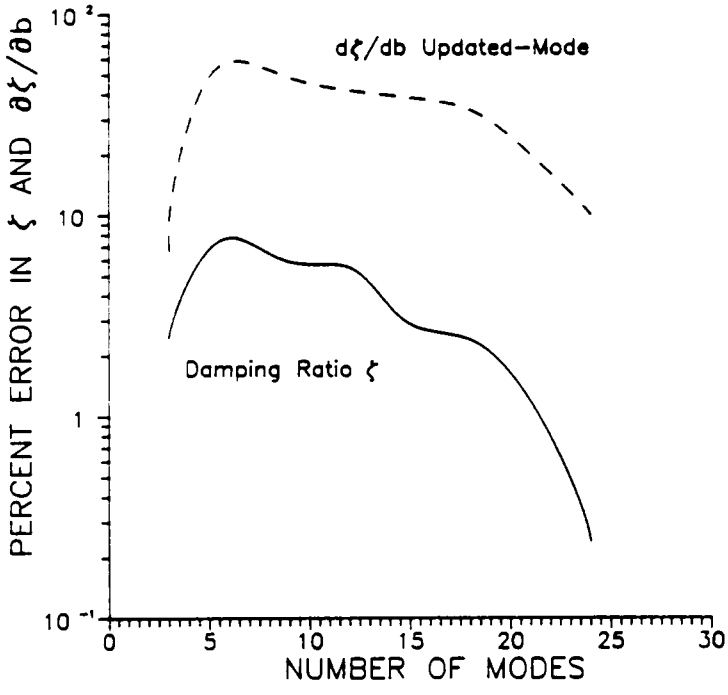

Figure 2.9: Convergence of Mode 2 Damping Ratio and its Derivative With Respect to Beam Width

2.5 Improved Convergence

The slow convergence of the derivative of the Fourier example is associated with the step discontinuity. To show that the slow convergence of the derivative of the damping ratios is associated with the discontinuities introduced by point damping,

the structure was reanalyzed with distributed damping. Rotation-rate controllers were used at every node and translation-rate controllers at every node except at the supports. Each type of controller has the same gain.

As before, the gains were designed to produce damping ratios between one and ten percent for the first 10 modes. This was accomplished with a translation-rate gain $d_1 = .0003$ lb-s/in and rotation-rate gain $d_2 = .024$ lb-in-s. Table 2.4 shows the full-model (30-element) damping ratios and derivatives of damping ratios with respect to an added mass at point A for the first 10 modes.

Table 2.4 : Damping Ratios and Derivatives — Distributed Damping

Mode	Damping Ratio	Derivative
1	0.0879556	-5.49551
2	0.0826721	-3.05576
3	0.0681830	-.487291
4	0.0558581	-5.28100
5	0.0464619	-3.27698
6	0.0540090	-3.36439
7	0.0532779	-3.38890
8	0.0480473	0.117153
9	0.0433969	-3.37636
10	0.0389295	-3.70461

Updated-mode derivatives were calculated for gradually increasing size models, and the errors in the damping ratios and derivatives were calculated with respect to the full-finite-element results. Figure 2.10 shows the convergence of the sixth damping ratio and its derivative (this derivative had the slowest convergence rate of the first six modes).

The damping ratio and derivative converge much faster than for the point-control case. With the distributed control, the worst-case derivative converges to

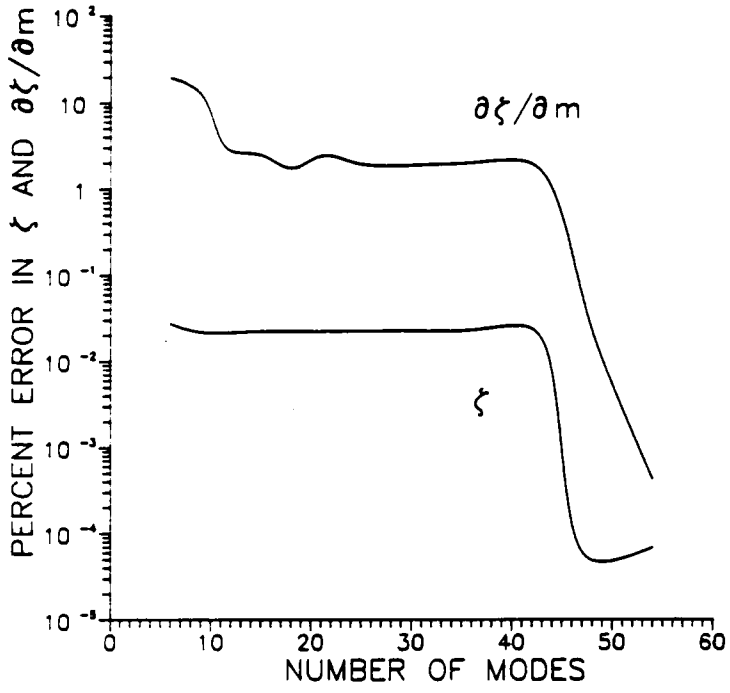

Figure 2.10: Convergence of Mode 4 Damping Ratio and its Derivative With Distributed Control

within 10% error with about 10 modes out of 56 total modes, where as in the point-control case, it took more than 90% of the available modes to achieve 10% accuracy, regardless of the original size of the finite-element model. Also, the damping ratio is essentially converged for the smallest model.

It has been shown that when obtaining an approximate solution to a dynamic system using mode superposition, an improved reduced-basis model can be formed by combining the vibration modes with Ritz vectors associated with the static response to the applied loads.[28,29] This accelerated convergence may be due to the static response vectors capturing the discontinuities associated with the loading. For the case of a point actuator, it may be similarly advisable to add the static response due to point loads at the actuator locations. Two Ritz vectors corresponding to the static response to a unit load at the translation-rate controller and a unit torque at the rotation-rate controller were added to the eigenvectors to

form the reduced model. Thus, for a six-mode model, the two Ritz vectors and the first four vibration modes were used to form the reduced model. The calculations for the reduced-model derivatives were the same as before except that the reduced mass and stiffness matrices were no longer diagonal.

Figure 2.11 shows the effect of the additional Ritz vectors on the convergence of the fourth damping ratio and its derivative (The errors are calculated with respect to the full-finite-element results). It can be seen that the convergence is greatly improved with the Ritz vectors for both the damping ratio and derivative. Without the Ritz vectors, there is a 36% error in the derivative with 24 out of 26 modes used. However, with the Ritz vectors included, the derivative converges to within 10% error with only 8 modes.

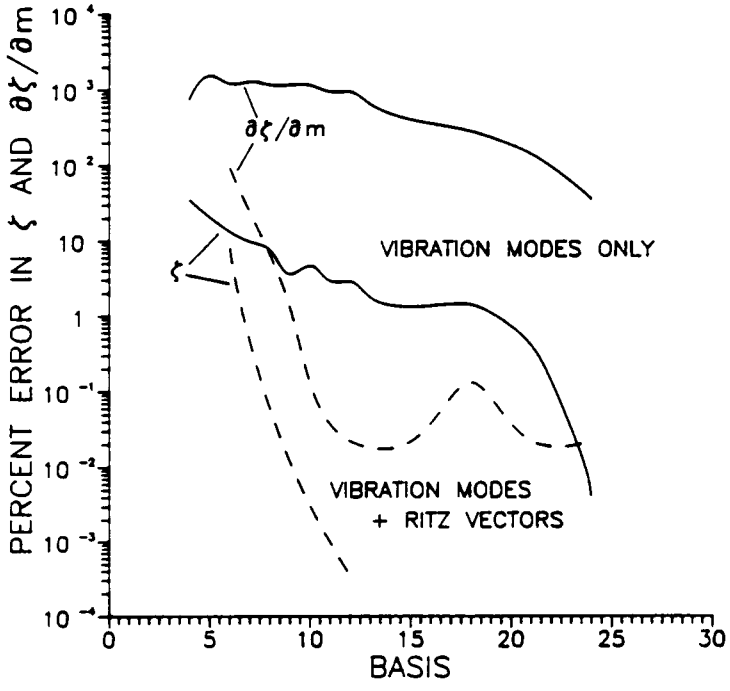

Figure 2.11: Convergence Comparison of Mode 4 Damping Ratio and its Derivative — Vibration Modes Only Vs. Vibration Modes + Ritz Vectors

The derivative was taken with respect to a mass located at the displacement-rate controller, thus it is possible to infer that the desired Ritz vector is associated with the mass rather than with the actuators. In order to separate the effects of the actuator Ritz vectors and the mass-location Ritz vector, the derivative with respect to an added mass located one-third span to the right of the rotation-rate controller (point B on Fig. 2.2) was calculated.

Reduced models of vibration modes only, vibration modes plus Ritz vectors corresponding to unit loads at actuator locations, and vibration modes plus a Ritz vector corresponding to a unit load at the added-mass location, are used to calculate the fixed-mode derivative. Figure 2.12 shows the convergence of the mode-5 derivative for the three models. As can be seen from the Figure, the Ritz vectors should be associated with the actuators rather than the point mass.

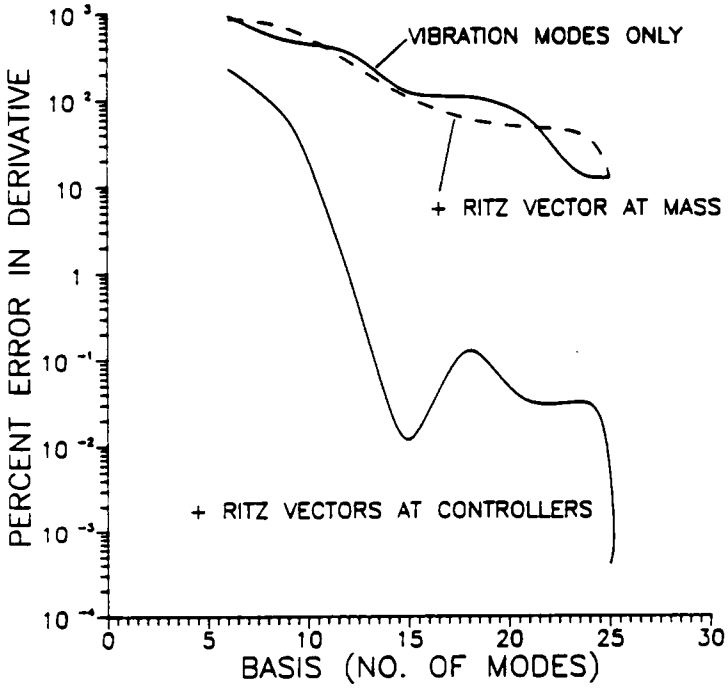

Figure 2.12: Effect of Ritz-Vector Locations on Convergence of Mode-5 Damping-Ratio Derivative

2.6 Concluding Remarks

Modal expansion is a generalization of the Fourier series. It is well known that Fourier series of discontinuous functions converge slowly and that the derivatives of the series may not converge at all. Accordingly, slow convergence of modal expansion can be expected when the applied loads exhibit discontinuities in time or space. In a controlled structure, where most of the damping is supplied by the control system, convergence problems may be caused by point actuators.

A multispan, simply-supported beam controlled with a direct-feedback control using point actuators was used to demonstrate that convergence problems due to point actuators do occur. The damping ratios and their derivatives with respect to an added mass were calculated using several finite-element models. Reduced models based on vibration modes were also formed and used to calculate the damping ratios and their derivatives. Fixed-mode and updated-mode derivative calculation procedures were investigated.

The results showed that errors in the reduced-model derivatives of the damping ratios were about an order of magnitude larger than the errors in the damping ratios themselves. Also, in the zone where the error in the derivatives was acceptable, there was no substantial difference between the fixed-mode derivatives and updated-mode derivatives, thus cheaper fixed-mode method is preferred.

To show that the slow convergence of the reduced-model derivatives was due to the point actuators, the beam was analyzed with distributed actuators. In the distributed-actuator case, the derivatives converged much faster.

The convergence of the derivatives with increasing number of modes was compared to the convergence with increasing number of finite-element degrees of freedom. For the derivative of the fourth damping ratio (point-actuator case), it was

found that the finite-element approximation converged faster than the modal approximation. This led to a paradoxical situation where improving the accuracy of the modes by using a finer finite-element mesh increased the error of the modal approximation. This indicates that in the case of point actuators, it may be impractical to use a modal approximation based solely on vibration modes to calculate derivatives of closed-loop response with respect to structural parameters.

In transient response problems, it is known that complementing the vibration modes with a mode representing static response to the loads can greatly improve convergence. Similarly, for the example studied, it was shown that if Ritz vectors corresponding to static responses due to unit loads at the actuators were added to the basis vectors, the convergence of the reduced-model derivatives was greatly enhanced. The only disadvantage of using the Ritz vectors is that the system matrices are no longer diagonal.

Chapter 3

Linear Quadratic Regulator

In Chapter 2, the effect of modal truncation on closed-loop damping ratios and their derivatives for a simple structure with a simple control system was investigated in great detail. The objective of this chapter is to verify the main results of Chapter 2 for a more complex control system. The control consists of a Linear Quadratic Regulator (LQR) coupled with a simple observer. The theory for the Linear Quadratic Regulator can be found in Reference 37.

The object is to verify the main results of the last chapter for a more complex control system, thus aspects concerning the different derivatives, derivative approximations, and finite-element meshes will not be discussed. It will be shown that the derivatives of closed-loop damping ratios with respect to an added mass converge much slower than their corresponding damping ratios and that Ritz vectors included in the reduced model accelerate convergence.

The same multispan beam will be used in this chapter; however, the units have been changed to metric to be compatible with the literature. The geometry has

also been changed in order to lower the natural frequencies of the structure, thus better simulating a flexible space structure.

3.1 Analysis and Sensitivity Calculations

3.1.1 *Equations of Motion*

The discretized equations of motion for a flexible structure with an output-feedback control are written

$$M\ddot{\mathbf{q}} + D\dot{\mathbf{q}} + K\mathbf{q} = U_c\mathbf{u} \tag{3.1}$$

where M, D, K, and U_c, are the mass, inherent damping, stiffness, and control influence matrices, respectively, $\mathbf{q}$ is the n degrees-of-freedom displacement vector, and $\mathbf{u}$ is a vector of control forces.

The order of the above equations is typically too large for designing a control system; therefore, the order of the model is reduced by expressing the displacement vector $\mathbf{q}$ as a linear combination of a small number of reduced-basis vectors by

$$\mathbf{q} = \Phi\eta \tag{3.2}$$

where Φ is a matrix whose columns are reduced-basis vectors and η is a vector of amplitudes. As in the previous chapter, Φ may contain both natural vibration modes and Ritz vectors corresponding to static displacements; however, for this derivation, they will all be referred to as modes and the amplitudes will be referred to as modal coordinates.

Substituting Eq. (3.2) into Eq. (3.1) and pre-multiplying by Φ^T gives us the equations in modal form

$$\hat{M}\ddot{\eta} + \hat{D}\dot{\eta} + \hat{K}\eta = \Phi^T U_c\mathbf{u} \tag{3.3}$$

where

$$\hat{M} = \Phi^T M \Phi \qquad \hat{D} = \Phi^T D \Phi \qquad \hat{K} = \Phi^T K \Phi \tag{3.4}$$

It is assumed that the inherent damping matrix D can be approximated as a linear combination of the mass and stiffness matrix, so that if Φ contains vibration modes only, then $\hat{D}$ is diagonal (as well as $\hat{M}$ and $\hat{K}$). Multiplying through by $\hat{M}^{-1}$,

$$\ddot{\eta} + \hat{M}^{-1}\hat{D}\dot{\eta} + \hat{M}^{-1}\hat{K}\eta = \hat{M}^{-1}\Phi^T U_c \mathbf{u} \tag{3.5}$$

Finally, in order to design and analyze the LQR control system, it is convenient to write Eq. (3.5) in state form as

$$\begin{Bmatrix} \ddot{\eta} \\ \dot{\eta} \end{Bmatrix} = \begin{bmatrix} -\hat{M}^{-1}\hat{D} & -\hat{M}^{-1}\hat{K} \\ I & 0 \end{bmatrix} \begin{Bmatrix} \dot{\eta} \\ \eta \end{Bmatrix} + \begin{bmatrix} \hat{M}^{-1}\Phi^T U_c \\ 0 \end{bmatrix} \mathbf{u}$$
$$\dot{\mathbf{x}} = A\mathbf{x} + B\mathbf{u} \tag{3.6}$$

where $\mathbf{x^T} = [\dot{\eta}^T \quad \eta^T]$.

The number of modes used in the reduced model determines the accuracy of the solution. It is assumed that n_c modes are used to design the control system, and then the response of the actual structure is approximated by analyzing it with additional modes. The modes with which the control system is designed are called the *controlled* modes and are denoted with a subscript c. The rest of the modes are called *residual* modes and are denoted with a subscript r. By appropriately partitioning Eq. (3.6), the state equation can be written in terms of controlled and residual modes as

$$\begin{Bmatrix} \dot{\mathbf{x}}_c \\ \dot{\mathbf{x}}_r \end{Bmatrix} = \begin{bmatrix} A_{cc} & A_{cr} \\ A_{rc} & A_{rr} \end{bmatrix} \begin{Bmatrix} \mathbf{x}_c \\ \mathbf{x}_r \end{Bmatrix} + \begin{bmatrix} B_c \\ B_r \end{bmatrix} \mathbf{u} \tag{3.7}$$

where

$$\mathbf{x}_c = [\dot{\eta}_1 \quad \dot{\eta}_2 \quad \dots \quad \dot{\eta}_c \quad \eta_1 \quad \eta_2 \quad \dots \quad \eta_c]^T \tag{3.8}$$

$$\mathbf{x_r} = \begin{bmatrix} \dot{\eta}_{c+1} & \dot{\eta}_{c+2} & \cdots & \dot{\eta}_r & \eta_{c+1} & \eta_{c+2} & \cdots & \eta_r \end{bmatrix}^T \tag{3.9}$$

If Φ contains only vibration modes, A_{cr} and A_{rc} are zero matrices.

3.1.2 *Control System Design*

The control system is a combination of a Linear Quadratic Regulator (LQR) and a simple observer. The regulator designed on the basis of a reduced model with n_c modes produces a control output $\mathbf{u}$ which minimizes the performance index

$$J = \int_0^\infty \left(\mathbf{x_c^T} Q \mathbf{x_c} + \mathbf{u^T} R \mathbf{u}\right) \, dt \tag{3.10}$$

where Q is a positive-semidefinite state-weighting matrix and R is a positive-definite control-weighting matrix. The unique control law that minimizes Eq. (3.10) is

$$\mathbf{u} = -R^{-1} B_c^T P_R \hat{\mathbf{x}}_\mathbf{c} = -G \hat{\mathbf{x}}_\mathbf{c} \tag{3.11}$$

where P_R is a constant, symmetric, positive-semidefinite matrix which satisfies the algebraic Riccati equation

$$A_{cc}^T P_R + P_R A_{cc} + Q - P_R B_c R^{-1} B_c^T P_R = 0 \tag{3.12}$$

and $\hat{\mathbf{x}}_\mathbf{c}$ is the current estimate of the state $\mathbf{x_c}$ based on the sensor measurements.

The sensors measure a subset of the full structural response, and for displacements, this subset can be written in modal form as

$$\mathbf{q_s} = \Phi_c^* \eta_\mathbf{c} + \Phi_r^* \eta_\mathbf{r} \tag{3.13}$$

where the asterisks represent modal matrices which include only the rows corresponding to the degrees of freedom which the sensors measure.

In *designing* the control system, the residual modes are neglected, thus the second term in Eq. (3.13) is ignored. This gives us

$$\hat{\eta}_c = \Phi_c^{*-1} q_s \tag{3.14}$$

Note, that since Φ_c is inverted, it must be square. This requires that there are as many sensors as controlled modes. The approximation shown in Eq. (3.14) has been called static observation[38,39] and modal filtering.[40]

When *analyzing* the effect of the control system on the full model, the residual modes must be included. Substituting Eq. (3.13) into Eq. (3.14), an expression for the observed modal coordinates can be written

$$\begin{aligned} \hat{\eta}_c &= \Phi_c^{*-1}[\,\Phi_c^* \quad \Phi_r^*\,]\eta \\ &= [\,I \quad \Phi_c^{*-1}\Phi_r^*\,]\eta \\ &= \Psi\eta \end{aligned} \tag{3.15}$$

One way to think of this is that the control system thinks it is sensing η_c but it is actually sensing $\hat{\eta}_c$, which is contaminated by the residual modes. An identical derivation gives us the observed modal velocities

$$\hat{\dot{\eta}}_c = \Psi\dot{\eta} \tag{3.16}$$

Looking at Eq. (3.14) it is seen that Φ_c^* can indicate whether a set of sensor locations is acceptable. Since Φ_c^* has to be inverted, it should be as far from singular as possible. By trying different sensor locations (i.e. choosing different combinations of rows for Φ_c^*) and calculating the condition number (the ratio of the largest to the smallest eigenvalue of a matrix) of Φ_c^*, *good* sensor locations can be determined. The observer will be more robust if the sensors are in good locations. The sensor locations are good if the condition number of Φ_c^* is small.

Substituting Eqs. (3.15) and (3.16) into Eq. (3.11), the control law can be written

$$\mathbf{u} = -G \begin{bmatrix} \Psi & 0 \\ 0 & \Psi \end{bmatrix} \begin{Bmatrix} \dot{\eta} \\ \eta \end{Bmatrix} \tag{3.17}$$

This can then be substituted into Eq. (3.6) to get the closed-loop system

$$\begin{Bmatrix} \ddot{\eta} \\ \dot{\eta} \end{Bmatrix} = \left[\begin{bmatrix} -\hat{M}^{-1}\hat{D} & -\hat{M}^{-1}\hat{K} \\ I & 0 \end{bmatrix} - \begin{bmatrix} \hat{M}^{-1}\Phi^T U_c \\ 0 \end{bmatrix} G \begin{bmatrix} \Psi & 0 \\ 0 & \Psi \end{bmatrix} \right] \begin{Bmatrix} \dot{\eta} \\ \eta \end{Bmatrix}$$
$$\dot{\mathbf{x}} = [A - BG\Psi^*]\mathbf{x} \tag{3.18}$$
$$\dot{\mathbf{x}} = \bar{A}\bar{\mathbf{x}}$$

3.1.3 *Derivative Calculation*

As in the previous chapter, the derivative of the damping ratios with respect to a concentrated mass is calculated assuming that the control is fixed. The eigenvalue problem for Eq. (3.18) and the eigenvalue for the adjoint system are written

$$\bar{A}\mathbf{u_k} = \lambda_k \mathbf{u_k} \tag{3.19}$$

$$\mathbf{v_k}^T \bar{A} = \lambda_k \mathbf{v_k}^T \tag{3.20}$$

where λ_k is the k^{th} eigenvalue and $\mathbf{u_k}$ and $\mathbf{v_k}$ are the k^{th} right and left eigenvectors of the closed-loop system, respectively. Eq. (3.19) can be written

$$(\bar{A} - \lambda_k I)\mathbf{u_k} = \mathbf{0} \tag{3.21}$$

Differentiating with respect to some structural parameter, we get

$$(\bar{A} - \lambda_k I)\mathbf{u_k}' + (\bar{A}' - \lambda_k' I)\mathbf{u_k} = \mathbf{0} \tag{3.22}$$

where the primes indicate derivatives with respect to the structural parameter. Multiplying by $\mathbf{v_k}^T$ and solving for λ_k', we get

$$\lambda_k' = \frac{\mathbf{v_k}^T \bar{A}' \mathbf{u_k}}{\mathbf{v_k}^T \mathbf{u_k}} \tag{3.23}$$

From Eq. (3.18), it can be seen that

$$\bar{A}' = A' - B'G\Psi^* \tag{3.24}$$

It is easy to show that for the fixed-mode derivative with respect to an added mass

$$A' = \begin{bmatrix} -\hat{M}'^{-1}\hat{D} & -\hat{M}'^{-1}\hat{K} \\ 0 & 0 \end{bmatrix} \tag{3.25}$$

and

$$B' = \begin{bmatrix} \hat{M}'^{-1}\Phi^T U_c \\ 0 \end{bmatrix} \tag{3.26}$$

For both of the above expressions, $\hat{M}'^{-1}$ is needed. Using the identity $\hat{M}\hat{M}^{-1} = I$, differentiating with respect to an added mass and solving for $\hat{M}'^{-1}$ results in

$$\hat{M}'^{-1} = -\hat{M}^{-1}\hat{M}'\hat{M}^{-1} \tag{3.27}$$

Expanding $\hat{M}'$, it is seen that

$$\hat{M}' = \Phi'^T M\Phi + \Phi^T M'\Phi + \Phi^T M\Phi' \tag{3.28}$$

Using the fixed-mode approximation, this reduces to

$$\hat{M}' = \Phi^T M'\Phi \tag{3.29}$$

As discussed in the previous chapter, the matrix M' is simply a zero matrix with a 1 on the diagonal at the location corresponding to the added mass.

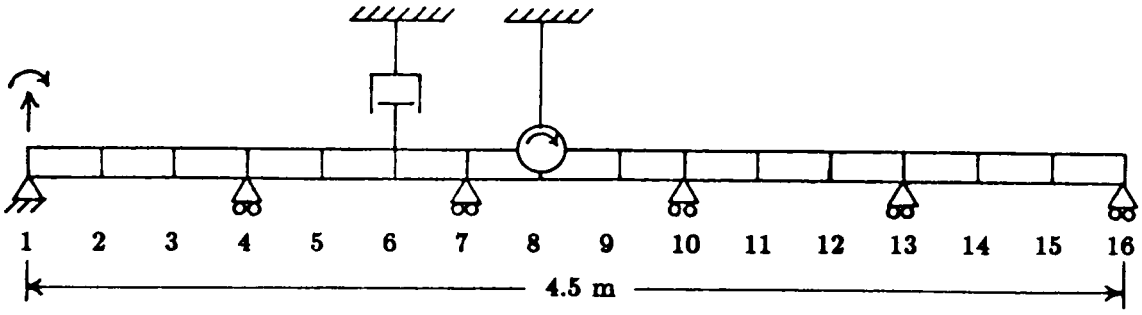

$A = 50\ \text{mm}^2$ $\quad \rho = 7.6 \times 10^4\ \text{N/m}^3$
$E = (10)^9\ \text{N/m}^2$ $\quad I = 4.167\ \text{mm}^4$

Figure 3.1: Multispan Beam Geometry

3.2 Multispan Beam Example

As stated earlier, the multispan beam of Chapter 2 was used with SI units employed. Also, some of the geometric and material variables were changed so that the natural frequencies would be lower, thus better representing a flexible space structure. The redesigned beam is shown in Figure 3.1.

The beam is again modeled with three cubic beam finite elements per span. Table 3.1 shows the natural frequencies for the first 10 out of 26 total modes.

Two rigidly-anchored, massless actuators were placed on the beam as shown in Figure 3.1; the first is a displacement actuator at node 6, and the second is a rotation actuator at node 8.

Several sensor location cases were evaluated for sensing the first five modes by looking at the condition number of Φ_c^* as described in the previous section. The resulting condition numbers ranged from 1 to 20, indicating that the condition number was not very sensitive to the sensor locations. However, the robustness of the observer depends on the condition number, thus the set of sensor locations should attempt to minimize the condition number. The only place a sensor can

not be placed is at a restrained degree of freedom, which would result in an infinite condition number.

The case chosen was translation sensors at nodes 6 and 12, and rotation sensors at nodes 1, 8, and 16. The condition number for this case was 1.3535. This set was chosen since the control system was stable for these sensor locations.

The control system is designed to produce damping ratios for the first five modes between 1% and 10%. This is accomplished using

$$Q = \frac{1}{2}\begin{bmatrix} \Phi_c^T K \Phi_c & 0 \\ 0 & \Phi_c^T K \Phi_c \end{bmatrix} \tag{3.30}$$

and $R = diag(25.0, \quad 25.0)$. Inherent damping of .001 is assumed for each mode. The damping ratios for the first ten modes are also given in Table 3.1 .

Table 3.1 : Natural Frequencies and Damping Ratios of Multispan Beam

Mode	Natural Frequency (Hz)	Damping Ratio
1	.201290	.094373
2	.223363	.052569
3	.279469	.084092
4	.352328	.088943
5	.423448	.019499
6	.814019	.001701
7	.861512	.039547
8	.970987	.001689
9	1.103073	.044838
10	1.225521	.010885

3.3 Convergence of Damping Ratios and Derivatives

3.3.1 *Reduced Models With Vibration Modes Only*

The damping ratios and their derivatives with respect to an added mass at node 9 are first calculated using reduced models that contain only vibration modes. The convergence histories are shown in Figures 3.2 and 3.3 for three controlled modes (modes 1, 3, and 5) and one residual mode (mode 7). Tables 3.2 and 3.3 contains the percent error in the damping ratios and derivatives, respectively, with respect to the full-model values.

Table 3.2 : Percent Error in Damping Ratios, Vibration Modes Only

Basis	ζ_1	ζ_3	ζ_5	ζ_7
5	52.5	143.4	1601.	
10	36.8	90.2	764.7	97.1
15	10.6	26.4	117.1	9.9
20	4.1	10.3	39.4	4.7
25	.77	1.92	6.3	.62

Table 3.3 : Percent Error in Derivatives, Vibration Modes Only

Basis	ζ_1'	ζ_3'	ζ_5'	ζ_7'
5	184.5	271.3	7.3×10^4	
10	117.5	370.8	4.0×10^4	152.0
15	32.8	99.9	2.69×10^3	200.0
20	12.6	33.1	634.0	83.3
25	2.4	5.1	69.5	14.7

Figure 3.2 shows that the damping ratios converge slowly. For example, in order to obtain 10% accuracy, 20 out of 26 modes are needed for ζ_3, and 23 modes are needed for ζ_5. This is in contrast to the rate-feedback case presented in Chapter 2,

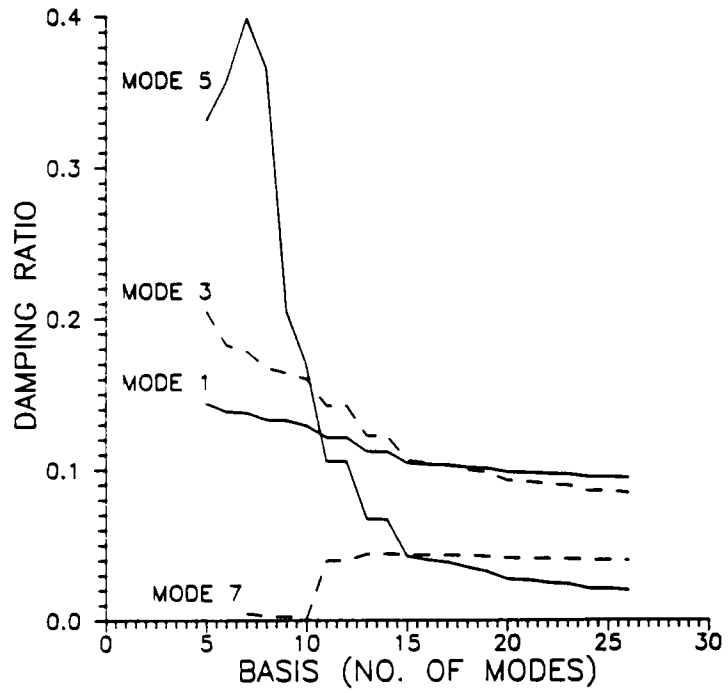

Figure 3.2: Convergence of Damping Ratios, Vibration Modes Only

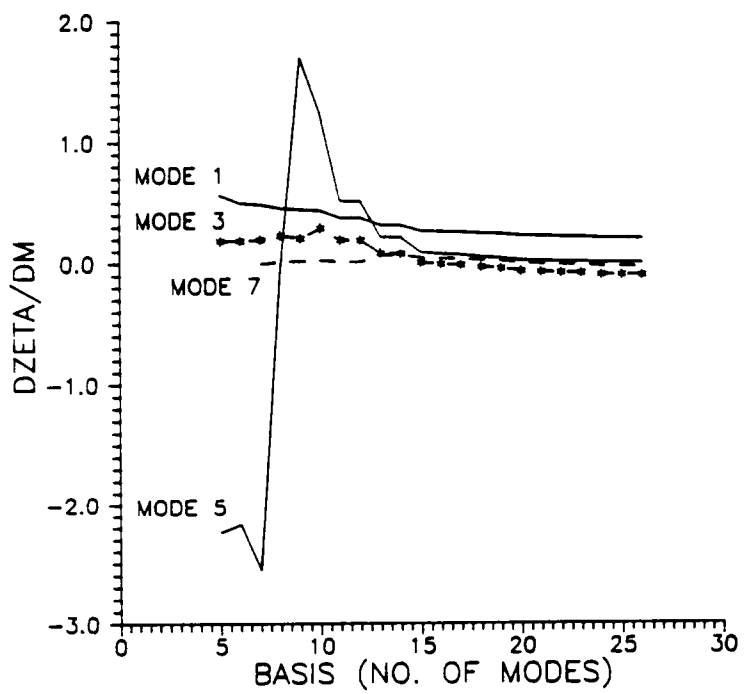

Figure 3.3: Convergence of Derivatives, Vibration Modes Only

where damping ratios converged to within 10% with between 10 and 15 modes. The reason for the difference is that the LQR control system is designed on the basis of a reduced model, whereas the rate-feedback system was designed using the full model.

Figure 3.3 shows the convergence of the derivatives. The convergence of mode 5 is so poor that it distorts the convergence of the rest of the modes; therefore, the convergence histories are repeated in Figure 3.4 on a smaller scale. One possible reason that mode 5 is so much worse than the others is that its full-model derivative is much smaller than the other full-model derivatives, thus making it sensitive to numerical error.

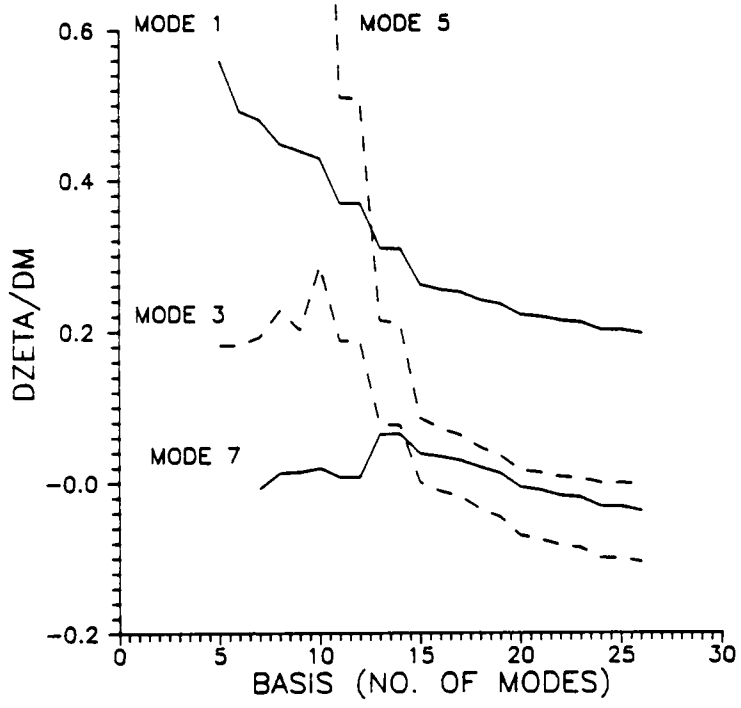

Figure 3.4: Convergence of Derivatives, Vibration Modes Only

From Figure 3.4, it is again obvious that the convergence of the derivatives is very poor. Both modes 5 and 7 do not converge to within 10% with 25 out of 26 modes, and with 23 modes, the error is 272% in mode 5 and 47% in mode 7. Also,

as shown in Chapter 2, the convergence of the derivatives is consistently slower than the convergence of the damping ratios.

3.3.2 *Reduced Models With Ritz Vectors and Vibration Modes*

Two Ritz vectors corresponding to static displacements due to unit loads at the actuator locations are calculated. Reduced models containing the Ritz vectors and vibration modes are formed. The only restriction is that the 5 controlled modes must be the first to be included in the model. For instance, a 10-mode model would include the first 5 vibration modes, the 2 Ritz vectors, then the next 3 vibration modes. The convergence of the damping ratios and their derivatives are shown in Figures 3.5 and 3.6 for modes 1, 3, 5, and 7, and the errors with respect to the full model values are shown in Tables 3.4 and 3.5.

Table 3.4 : Percent Error in Damping Ratios, With Ritz Vectors

Basis	ς_1	ς_3	ς_5	ς_7
5	52.5	143.4	1601.	
10	.0138	.0107	1.99	4.09
15	0	.0012	.041	.0329
20	0	.0012	0	.0025
25	0	0	0	0

Table 3.5 : Percent Error in Derivatives, With Ritz Vectors

Basis	ς_1'	ς_3'	ς_5'	ς_7'
5	184.5	271.3	7.3×10^4	
10	1.026	3.396	702.8	85.84
15	.1545	.0264	9.409	.3567
20	.0417	.0217	5.946	.1075
25	.0041	.0047	1.241	.0184

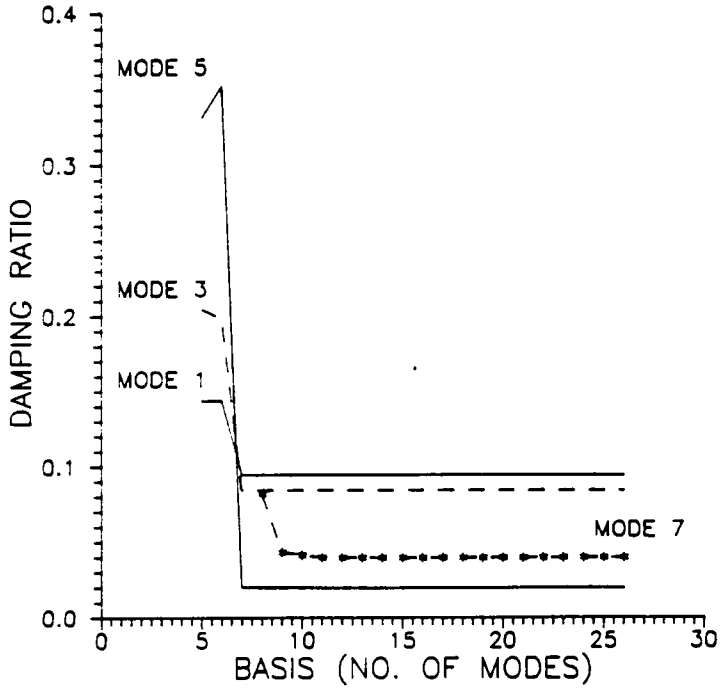

Figure 3.5: Convergence of Damping Ratios, With Ritz Vectors

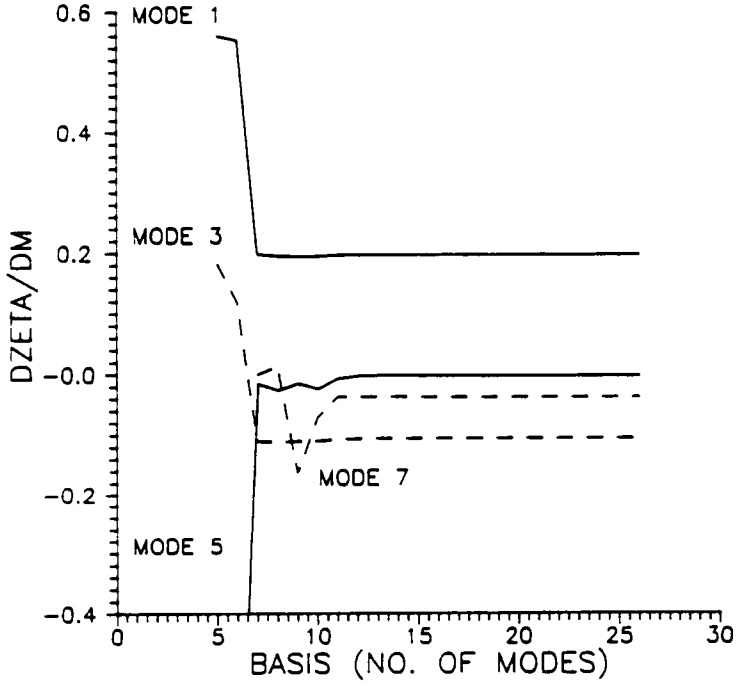

Figure 3.6: Convergence of Derivatives, With Ritz Vectors

As seen from the Figures, both the damping ratios and derivatives are essentially converged with 10 modes. The only exception is the derivative of mode 5, which requires 15 modes to converge to within 10%. As stated before, this is probably due to the relative size of the derivative.

3.4 Concluding Remarks

The main results of Chapter 2 have been shown to hold true for an LQR control system. It was shown that the derivatives converge slower than the damping ratios. In addition, it was shown that the damping ratios also converged slowly. This is due to the control system being designed on the basis of a reduced model.

It was shown that Ritz vectors added to the reduced model dramatically improved the convergence of both the damping ratios and their derivatives.

Chapter 4

Linear Quadratic Gaussian Control

In the previous chapter, the control system investigated consisted of a LQ regulator and a modal filter. In this chapter, the complexity and efficiency of the system is increased by replacing the modal filter with an optimal Kalman filter. The Kalman filter reconstructs the full state from a limited number of measured states, and unlike the modal filter, the number of sensors can be different from the number of controlled modes. The combined LQR and Kalman filter is referred to as a Linear Quadratic Gaussian (LQG) control system.[37]

In the first part of the chapter, the analyses of the previous chapters is repeated on the same simply-supported beam using the LQG control system. The convergence of the damping ratios and their derivatives are examined for reduced models containing vibration modes only and reduced models that contain both vibration modes and Ritz vectors.

In the second part of the chapter, the effect the Ritz vectors have on the design of the control system is examined. When a control system is designed with a reduced model, and then analyzed with the full model, it is often found that the

damping predicted by the reduced model is not realized in the full model. This damping shortfall is investigated for control systems designed with reduced models based on vibration modes only and for control systems designed with reduced models that include Ritz vectors.

4.1 Analysis and Sensitivity Calculations

For convenience, a derivation of the LQG problem and sensitivity analysis is presented here even though some of the equations have been presented in the previous chapters.

4.1.1 *Equations of Motion*

As before the discretized equations of motion for a flexible structure with an output-feedback control are written

$$M\ddot{\mathbf{q}} + D\dot{\mathbf{q}} + K\mathbf{q} = U_c\mathbf{u} \tag{4.1}$$

where M, D, K, and U_c, are the mass, inherent damping, stiffness, and control influence matrices, respectively, $\mathbf{q}$ is the n degrees-of-freedom displacement vector, and $\mathbf{u}$ is a vector of control forces. To effect the control, it is assumed that n_s velocities are measured, and the sensed velocity $\mathbf{y}$ can be written as

$$\mathbf{y} = U_s\dot{\mathbf{q}} \tag{4.2}$$

where U_s is the sensor influence matrix.

Applying modal reduction to Eq. (4.1), and simplifying, we get

$$\ddot{\eta} + \hat{M}^{-1}\hat{D}\dot{\eta} + \hat{M}^{-1}\hat{K}\eta = \hat{M}^{-1}\Phi^T U_c\mathbf{u} \tag{4.3}$$

In order to design and analyze the LQG control system, it is convenient to write Eq. (4.3) in state form as

$$\begin{Bmatrix} \ddot{\eta} \\ \dot{\eta} \end{Bmatrix} = \begin{bmatrix} -\hat{M}^{-1}\hat{D} & -\hat{M}^{-1}\hat{K} \\ I & 0 \end{bmatrix} \begin{Bmatrix} \dot{\eta} \\ \eta \end{Bmatrix} + \begin{bmatrix} \hat{M}^{-1}\Phi^T U_c \\ 0 \end{bmatrix} \mathbf{u} \tag{4.4}$$
$$\dot{\mathbf{x}} = A\mathbf{x} + B\mathbf{u}$$

where $\mathbf{x}^T = [\dot{\eta}^T \quad \eta^T]$.

By appropriately partitioning Eq. (4.4) the state equation can be written in terms of controlled and residual modes as

$$\begin{Bmatrix} \dot{\mathbf{x}}_c \\ \dot{\mathbf{x}}_r \end{Bmatrix} = \begin{bmatrix} A_{cc} & A_{cr} \\ A_{rc} & A_{rr} \end{bmatrix} \begin{Bmatrix} \mathbf{x}_c \\ \mathbf{x}_r \end{Bmatrix} + \begin{bmatrix} B_c \\ B_r \end{bmatrix} \mathbf{u} \tag{4.5}$$

If Φ contains only vibration modes, A_{cr} and A_{rc} are zero matrices.

Equation (4.2) can be transformed to modal coordinates and written in state form as

$$\mathbf{y} = U_s \Phi \dot{\eta} = C\mathbf{x} = [\, C_c \quad C_r \,] \begin{Bmatrix} \mathbf{x}_c \\ \mathbf{x}_r \end{Bmatrix} \tag{4.6}$$

4.1.2 *Control System Design*

The Linear Quadratic Gaussian (LQG) compensator combines a Linear Quadratic regulator and a Kalman filter. The regulator designed on the basis of a reduced model with n_c modes produces a control output $\mathbf{u}$ which minimizes the performance index

$$J = \int_0^\infty \left(\mathbf{x}_c^T Q \mathbf{x}_c + \mathbf{u}^T R \mathbf{u} \right) dt \tag{4.7}$$

where Q is a positive-semidefinite state-weighting matrix and R is a positive-definite control-weighting matrix. The unique control law that minimizes Eq. (4.7) is

$$\mathbf{u} = -R^{-1} B_c^T P_R \hat{\mathbf{x}}_c = -G\hat{\mathbf{x}}_c \tag{4.8}$$

where P_R is a constant, symmetric, positive-semidefinite matrix which satisfies the algebraic Riccati equation

$$A_{cc}^T P_R + P_R A_{cc} + Q - P_R B_c R^{-1} B_c^T P_R = 0 \tag{4.9}$$

and $\hat{\mathbf{x}}_\mathbf{c}$ is the current estimate of the state $\mathbf{x_c}$ based on the measurement $\mathbf{y}$. This estimate is produced by the Kalman filter, which is defined by the equation

$$\dot{\hat{\mathbf{x}}}_\mathbf{c} = A_{cc}\hat{\mathbf{x}}_\mathbf{c} + B_c\mathbf{u} + K_f(\mathbf{y} - C_c\hat{\mathbf{x}}) \tag{4.10}$$

where the filter gain matrix K_f is given by

$$K_f = P_F C_c^T V_2^{-1} \tag{4.11}$$

where P_F is the constant, symmetric, positive-semidefinite matrix which satisfies the algebraic Riccati equation

$$(A_{cc} + \alpha I)P_F + P_F(A_{cc} + \alpha I) - P_F C_c^T V_2^{-1} C_c P_F + V_1 = 0 \tag{4.12}$$

The matrices V_1 and V_2 represent the system and measurement noise, respectively. Since the details of the noise are generally not known, V_1 and V_2 are often used as design variables for the observer (e.g. Ref. 12). The constant α is used to enforce a predetermined degree of stability to the observer poles.[41] By adjusting V_1, V_2, and α, the observer can be designed to satisfy a rule of thumb that requires the observer poles to be between three and ten times faster (i.e. farther left in the imaginary plane) than the regulator poles. This produces an observer that is fast enough to reconstruct the regulator state, yet slow enough not to be overly sensitive to measurement noise.

In order to analyze the combined regulator/observer system using residual modes, it is convenient to introduce the estimator error

$$\mathbf{e_c} = \hat{\mathbf{x}}_\mathbf{c} - \mathbf{x_c} \tag{4.13}$$

The full, closed-loop system with both controlled and residual modes can now be written

$$\begin{Bmatrix} \dot{\mathbf{x}}_\mathbf{c} \\ \dot{\mathbf{e}}_\mathbf{c} \\ \dot{\mathbf{x}}_\mathbf{r} \end{Bmatrix} = \begin{bmatrix} A_{cc} - B_cG & -B_cG & A_{cr} \\ 0 & A_{cc} - K_fC_c & K_fC_r - A_{cr} \\ A_{rc} - B_rG & -B_rG & A_{rr} \end{bmatrix} \begin{Bmatrix} \mathbf{x}_\mathbf{c} \\ \mathbf{e}_\mathbf{c} \\ \mathbf{x}_\mathbf{r} \end{Bmatrix} = \bar{A}\bar{\mathbf{x}} \tag{4.14}$$

The closed-loop poles of Eq. (4.14), which are the eigenvalues of $\bar{A}$, can be written

$$\lambda_k = \sigma_k + i\omega_k \qquad k = 1, 2, \ldots, 4n_c + 2n_r \tag{4.15}$$

where σ_k and ω_k are the real and imaginary parts of the eigenvalues. The damping ratios are again used to represent the performance of the control system.

4.1.3 *Derivative Calculation*

In this chapter, the derivative of the damping ratio with respect to some structural parameter is again examined. Differentiating Eq. (4.15) with respect to some structural parameter, the derivative of the damping ratio is obtained as

$$\varsigma_k' = \frac{\omega_k(\sigma_k\omega_k' - \omega_k\sigma_k')}{(\sigma_k^2 + \omega_k^2)^{3/2}} \tag{4.16}$$

where primes denote derivatives with respect to the parameter. To evaluate Eq. (4.16), the derivatives of the closed-loop eigenvalues are needed, which, as shown in Chapter 3, can be calculated by

$$\lambda_k' = \frac{\mathbf{v_k}^T \bar{A}' \mathbf{u_k}}{\mathbf{v_k}^T \mathbf{u_k}} \tag{4.17}$$

where $\mathbf{u_k}$ and $\mathbf{v_k}$ are the left and right eigenvectors of the closed-loop system [Eq. (4.14)].

To calculate $\bar{A}'$, A, B, and C are differentiated before they are split into controlled and residual modes. Once the derivatives are calculated, they can again be partitioned into the form of Eq. (4.14). Differentiating A, we obtain

$$A' = \begin{bmatrix} -\hat{M}'^{-1}\hat{D} - \hat{M}^{-1}\hat{D}' & -\hat{M}'^{-1}\hat{K} - \hat{M}^{-1}\hat{K}' \\ 0 & 0 \end{bmatrix} \tag{4.18}$$

In this study, the structural parameter is an added concentrated mass, thus the terms $\hat{D}'$ and $\hat{K}'$ are both zero. The only derivative left is $\hat{M}'^{-1}$. As seen in Chapter 3, this is evaluated using the fixed-mode approximation as

$$\hat{M}'^{-1} = -\hat{M}^{-1}\Phi^T M' \Phi \hat{M}^{-1} \tag{4.19}$$

This now gives us all the ingredients needed to evaluate A'.

Following the same procedure, the derivative of B is found to be

$$B' = \begin{bmatrix} \hat{M}'^{-1}\Phi^T U_c \\ 0 \end{bmatrix} \tag{4.20}$$

and $C' = 0$.

Partitioning the above matrix derivatives, the derivative of $\bar{A}$ with respect to an added mass can now be written

$$\bar{A}' = \begin{bmatrix} A'_{cc} - B'_c G & -B'_c G & A'_{cr} \\ 0 & A'_{cc} & -A'_{cr} \\ A'_{rc} - B'_r G & -B'_r G & A'_{rr} \end{bmatrix} \tag{4.21}$$

4.2 Convergence of Damping Ratios and Derivatives

The simply-supported, multispan beam investigated in the previous chapters is again used for this chapter. The actuators are in the same locations as before, and as in Chapter 2, there are two rate sensors colocated with the actuators. Each mode is assumed to have .1% inherent damping.

An additional complexity in the LQG control is that the closed-loop system contains both regulator poles and observer poles. In this study, the regulator poles are of concern; however, when looking at the closed-loop eigenvalues, it is not always possible to distinguish the regulator poles from the observer poles. A procedure was therefore developed for keeping track of the regulator poles as the residual modes are added to the system.

An augmented closed-loop system matrix is defined as

$$\bar{C} = \bar{A} - \beta \bar{B} \tag{4.22}$$

where

$$\bar{B} = \begin{bmatrix} 0 & 0 & 0 \\ 0 & 0 & K_f C_r \\ -B_r G & -B_r G & 0 \end{bmatrix} \tag{4.23}$$

The $\bar{B}$ matrix contains the coupling terms between the regulator and observer; therefore, if the eigenvalues of $\bar{C}$ are evaluated with $\beta = 1$, the results will always include the original regulator poles, the original observer poles, and the eigenvalues corresponding to the residual modes with assumed damping of .1%. The regulator poles can be easily identified since they are originally well separated from the observer poles and the residual-mode eigenvalues. The value of β is then gradually varied from 1 to 0, and the regulator poles can be traced by using the last two regulator poles to predict the next one. The only requirement on β is that the first

step is small enough so that the regulator poles do not change position with respect to the rest of the eigenvalues. In this study, $\beta_i = 1 - 2^{i-12}$ for $i = 0, 1, \ldots, 12$.

This process of tracing the regulator poles needs to be performed each time a residual mode is added. However, in this study, it was found that after a certain number of residual modes were added, the regulator poles did not change position from the previous closed-loop solution with one less residual mode, thus the tracing after that point was not necessary.

The control system is designed using the first five modes so that, as in the previous chapters, the full-model damping ratios are between 1% and 10%. This is accomplished by designing the regulator using

$$Q = \frac{1}{2}\begin{bmatrix} \Phi_c^T K \Phi_c & 0 \\ 0 & \Phi_c^T K \Phi_c \end{bmatrix} \tag{4.24}$$

and $R = \text{diag}(45.0, \quad 45.0)$. The observer is designed so that the observer poles would satisfy the 3-to-10 rule-of-thumb discussed earlier. This is accomplished with $V_1 = V_2 = I$ and $\alpha = 0.95$. Table 4.1 shows the regulator poles and damping ratios obtained from both the initial, five-mode reduced model, and the full 26-mode model. As the Table shows, the initial regulator poles vary by as much as 500% from their corresponding full-model damping ratios.

Table 4.1 : Control Design and Full-Model Damping Ratios

Mode	Regulator Poles	ς	Observer Poles	Full-Model ς
1	(-.15216,1.2748)	.11853	(-1.9362,1.3799)	.07707
2	(-.07163,1.4041)	.05095	(-1.9667,1.4361)	.03172
3	(-.29017,1.7570)	.16294	(-2.0119,2.1487)	.06367
4	(-.17675,2.2313)	.07897	(-2.8198,2.0202)	.06204
5	(-.63044,2.5410)	.24081	(-5.6054,3.3409)	.03867

4.2.1 *Reduced Models with Vibration Modes Only*

The damping ratios and their derivatives with respect to an added mass at the translation controller are first calculated with the five controlled modes. The residual vibration modes are then added one at a time and the damping ratios and derivatives are again calculated. Figures 4.1 and 4.2 show the convergence of the first 5 damping ratios and their derivatives versus the number of total modes used in the model. Tables 4.2 and 4.3 show the percent errors with respect to full-model values in the damping ratios and derivatives, respectively.

Table 4.2 : Percent Error in Damping Ratios, Vibration Modes Only

Basis	ς_1	ς_2	ς_3	ς_4	ς_5
5	53.79	60.62	155.9	27.29	552.7
10	39.22	46.26	105.1	9.95	167.0
15	10.29	16.76	29.81	2.42	31.49
20	3.93	7.04	11.75	1.03	11.88
25	.79	1.28	2.31	.13	2.24

Table 4.3 : Percent Error in Derivatives, Vibration Modes Only

Basis	ς_1'	ς_2'	ς_3'	ς_4'	ς_5'
5	71.28	238.8	129.0	345.5	21.32
10	49.40	297.9	203.6	190.4	76.89
15	12.36	113.3	60.12	102.4	106.8
20	19.28	137.8	67.32	61.83	78.80
25	1.60	13.35	6.94	1.72	1.30

The damping ratios seem to converge fairly quickly up to about 15 modes and then slow down considerably. At 15 modes, both modes 3 and 5 have errors of about 30%. This convergence is slower than for the rate-feedback case in Chapter 2, where with 15 modes, the damping ratios had converged to within 10%.

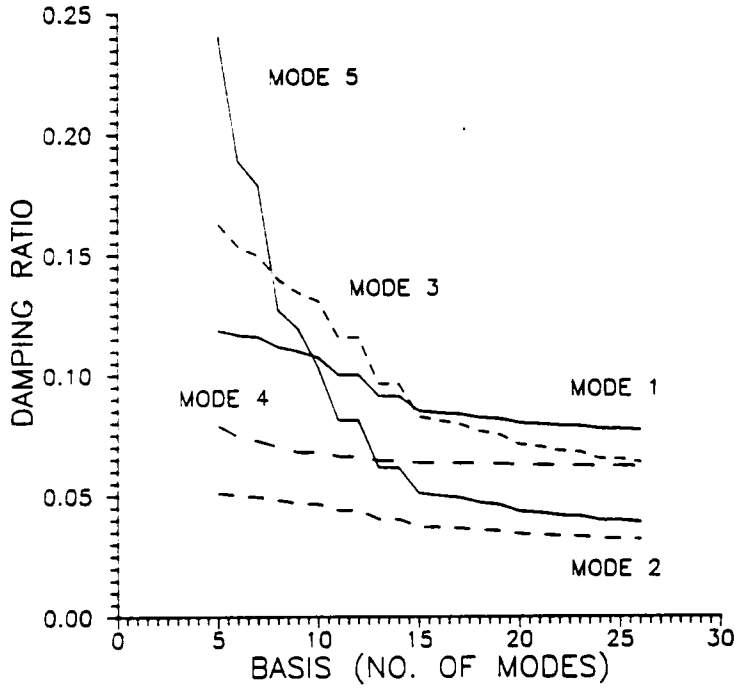

Figure 4.1: Convergence of Damping Ratios, Vibration Modes Only

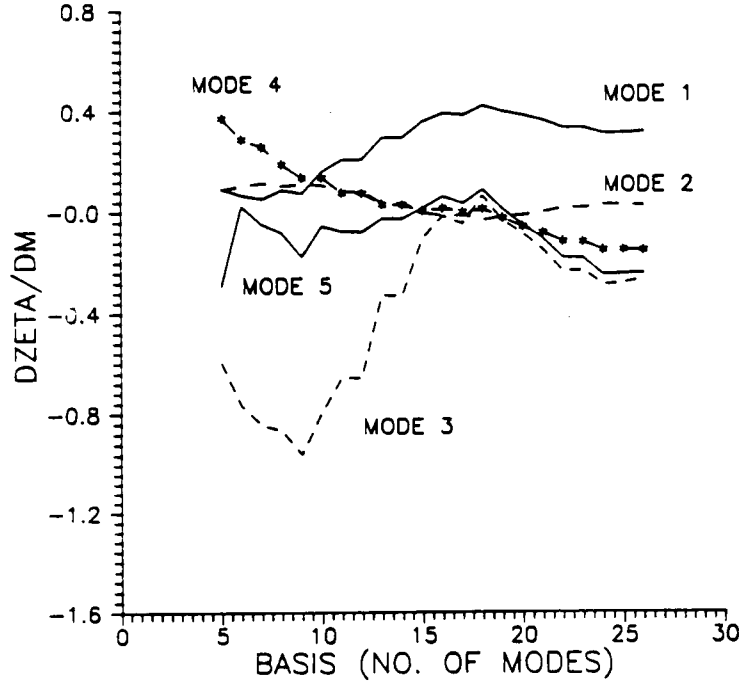

Figure 4.2: Convergence of Derivatives, Vibration Modes Only

In Figure 4.2, it is seen that the derivatives converge more slowly than the damping ratios. With a model of 15 modes, the error in derivatives of damping ratios of modes 2, 4, and 5 is still larger than 100%. With 23 out of 26 total modes, the errors in the same derivatives are larger than 20%, while the damping ratios have converged to within 10%.

4.2.2 *Reduced Models with Vibration Modes and Ritz Vectors*

In the previous chapters, the Ritz vectors were normalized so that the maximum term in each vector was 1. For the LQG control system, this will not work. The Ritz vectors contain large contributions from the lower modes, thus when they are added as residual modes, the physical control is changed.

The physical control force $\mathbf{u}$ is given by Eq. (4.8), where G is a fixed gain matrix and $\hat{\mathbf{x}}_c$ is the current estimate of the state produced by the Kalman filter. In a physical implementation, the Kalman filter equation [Eq. (4.10)] would be integrated to find $\hat{\mathbf{x}}_c$. If a Ritz vector is added without first making it orthogonal to the controlled modes, the modal mass matrix $\hat{M}$ will no longer be diagonal. This will change A_{cc} via Eq. (4.4), which in turn changes the state estimation produced by the observer. Finally, this will change the physical control $\mathbf{u}$. Therefore, since the control system is to remain fixed, the Ritz vectors must be made orthogonal to the controlled modes.

Letting $\mathbf{v}$ denote a Ritz vector, it is easy to show that a Ritz vector made orthogonal to n_c modes is given by

$$\bar{\mathbf{v}} = \mathbf{v} - \sum_{i=1}^{n_c} \alpha_i \boldsymbol{\phi}_i \tag{4.25}$$

where

$$\alpha_i = \mathbf{v}^T M \boldsymbol{\phi}_i \tag{4.26}$$

After the Ritz vectors have been made orthogonal to the controlled modes, the convergence study is repeated as before, except that the two Ritz vectors are the first to be added as residual modes. The results of the convergence studies are shown in Figures 4.3 and 4.4. Tables 4.4 and 4.5 show the percent errors with respect to full-model values in the damping ratios and derivatives, respectively.

Table 4.4 : Percent Error in Damping Ratios, With Ritz Vectors

Basis	ς_1	ς_2	ς_3	ς_4	ς_5
5	53.79	60.62	155.9	27.29	552.7
10	.0014	.0060	.0145	.0068	.0763
15	.0004	.0022	.0005	.0021	.0034
20	0	.0013	.0008	.0006	.0016
25	.0003	.0006	.0011	.0004	.0008

Table 4.5 : Percent Error in Derivatives, With Ritz Vectors

Basis	ς_1'	ς_2'	ς_3'	ς_4'	ς_5'
5	71.28	238.8	129.0	345.5	21.32
10	18.19	230.1	77.88	50.25	73.90
15	1.655	25.10	7.943	5.367	7.665
20	2.431	23.03	8.830	5.253	8.141
25	.0211	.1559	.0632	.0360	.0603

Figure 4.3 shows a dramatic improvement in the convergence of the damping ratios. With only the five controlled modes plus two Ritz vectors, the damping ratios are essentially converged. The convergence of the derivatives with the Ritz vectors is not as good, but is still better than in the vibration-modes-only case. The reason for the improvement in both the damping ratio and derivative is that the higher modes are needed to model the spatial discontinuity of the actuator forces rather than high-frequency actuator action. With the Ritz vectors correctly

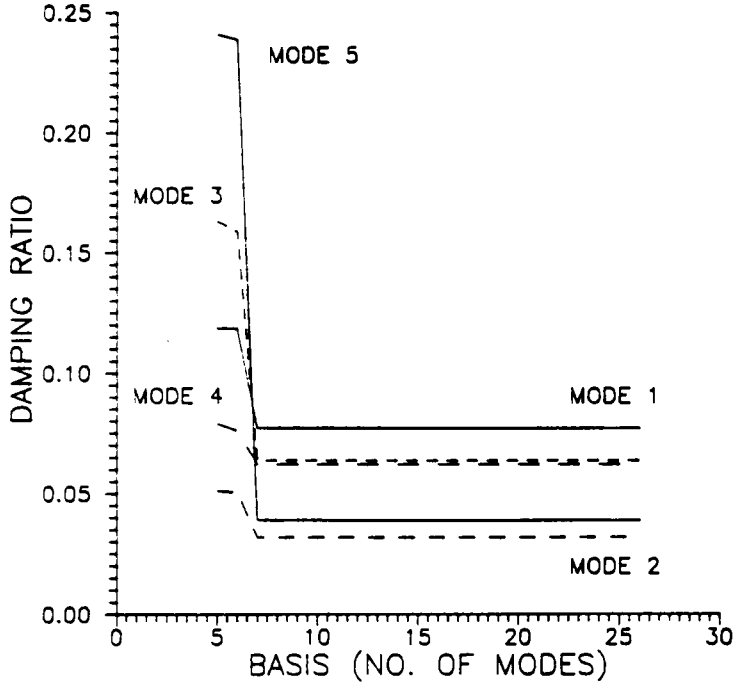

Figure 4.3: Convergence of Damping Ratios, With Ritz Vectors

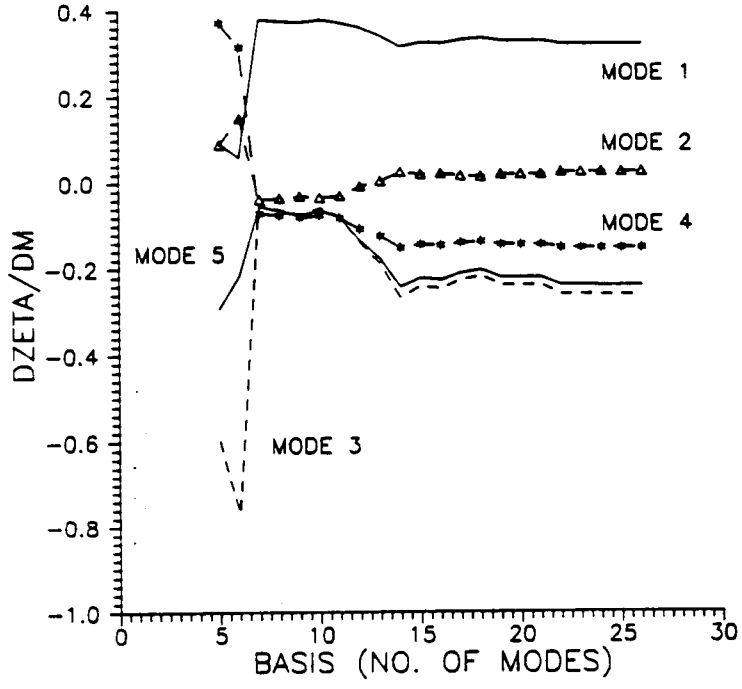

Figure 4.4: Convergence of Derivatives, With Ritz Vectors

modeling the spatial distribution of the response to actuator forces, there is no need for the higher modes.

4.3 Ritz Vectors in Control Design

Since the Ritz vectors accelerate the convergence of the reduced model to the full model, it may be useful to include them in the reduced model used for the control system design. This section considers this possibility.

It is assumed that a small number n_{c1} of modes are to be controlled, but in order to get a good design, a larger number of modes need to be included in the reduced model; that is $n_c > n_{c1}$. Thus the case where the additional modes are vibration modes is compared to the case where the additional modes are Ritz vectors.

Using the same structure and actuator/sensor locations, $n_{c1} = 3$ is selected, that is a control system that controls the first three vibration modes is designed. It has already been seen from the previous example that more than 3 modes are needed in the control design to insure that the damping ratios predicted by the reduced model are close to the actual damping ratios for the first three modes. The regulator and observer are designed to control the first three modes. Thus the regulator is designed with

$$Q = \frac{1}{2}\begin{bmatrix} \Phi_c^T K \Phi_c W & 0 \\ 0 & \Phi_c^T K \Phi_c W \end{bmatrix} \tag{4.27}$$

where $W = \text{diag}(3.0, \quad 15.0, \quad 2.0, \quad .01, \quad .01, \quad \ldots)$, and $R = \text{diag}(900, \quad 900)$. The observer is designed with $V_1 = \text{diag}(1.0, \quad 1.0, \quad 1.0, \quad 0.01, \quad 0.01, \quad \ldots, \quad 1.0, \quad 1.0, \quad 1.0, \quad 0.01, \quad 0.01, \quad \ldots)$, $V_2 = I$, and $\alpha = 0.69$. Designs are obtained with n_c of 5, 10, and 15 vibration modes.

For comparison, the control system is designed using 3 vibration modes plus 2 Ritz vectors, with R, V_2, and α the same, $W = \text{diag}(3.0, \quad 15.0, \quad 2.0, \quad 1.0, \quad .05)$, and $V_1 = \text{diag}(1.0, \quad 1.0, \quad 1.0, \quad 1.0, \quad 0.002)$. As before, the Ritz vectors must be modified to be acceptable to the LQG control system. First, the Ritz vectors are orthogonalized with respect to the three controlled modes. Then they are made orthogonal to each other and normalized to unit mass. As before, the residual modes must be orthogonal to the controlled modes, which means that the residual modes must be made orthogonal to the modified Ritz vectors.

Table 4.6 shows the results of the initial control design and full model damping ratios for modes 1, 2, and 3. The columns labeled 5, 10, and 15 are the 5-mode, 10-mode, and 15-mode control designs, and the column labeled $3+2$ is the control design using 3 vibration modes and 2 Ritz vectors.

Table 4.6 : Comparison of Control Designs: Damping Ratio Convergence

		5	10	15	3 + 2
ς_1	Control Design	.053257	.053265	.053264	.053205
	Full Model	.040325	.042201	.048682	.053213
ς_2	Control Design	.048571	.048588	.048587	.048420
	Full Model	.028116	.032910	.043238	.048666
ς_3	Control Design	.058766	.058811	.058808	.058491
	Full Model	.043177	.044472	.054168	.058794

From the Table, it is seen that even with 15 vibration modes in the controlled system, the actual damping ratios are not accurately represented by the reduced model. For example, when using 15 vibration modes to design the control system, the difference between the control-design and the actual damping is 12% for mode 2. However, for the case where the Ritz vectors are added to the 3 vibration modes, the

control-design damping ratios approximate the actual, full-model damping ratios to within 1%.

4.4 Concluding Remarks

In this chapter, an optimal control system consisting of an Linear Quadratic regulator and a Kalman filter was investigated using reduced models to both analyze the control performance and design the control system. In the analysis, it was found that both the damping ratios and derivatives converge slowly, but with the derivatives converging more slowly than the damping ratios. However, it was shown that when Ritz vectors corresponding to static displacements due to actuator forces are added to the reduced model, the convergence of both the damping ratios and their derivatives was accelerated.

It was also shown that the accuracy of the damping ratio predicted by a reduced-model control design can be significantly improved if the Ritz vectors are included in the design of the control system.

Thus it appears that Ritz vectors added to the reduced model of flexible structures can greatly improve the accuracy of both the design and analysis of the structure with a control system.

Chapter 5

Concluding Remarks

This dissertation has examined the effect of modal truncation on the analysis of three different active control systems for a simple multispan beam. It was shown that for all of the control systems, the derivatives of the damping ratios with respect to structural parameters converge much more slowly than their corresponding damping ratios. In the cases where the control system was designed on the basis of a reduced model, the damping ratios were also shown to converge slowly, thus indicating that the reduced-model control design does not accurately reflect the actual control on the structure. These results indicate that reduced models based solely on vibration modes are not adequate for calculating control performance or derivatives of control performance with respect to structural parameters for flexible structures with point actuators.

Ritz vectors corresponding to static displacements due to unit loads at the actuators were shown to improve the reduced models. It was shown that the accuracy of both the damping ratios and their derivatives were greatly improved when Ritz vectors were added to the model. This indicates that when analyzing a

flexible structure with point actuators, Ritz vectors should be added to the reduced model in order to capture the motions caused by the actuators. It was also shown that if the Ritz vectors were added to the reduced model for the design of the control system, the resulting control design more accurately predicted the control on the full structure.

Further research in this area could include the elimination of the spillover in the LQG case. This may be accomplished by adding or moving sensors and actuators, or by changing some of the control and observer weighting matrices. Also, the results should be verified for a more realistic three-dimensional structure.

References

1. Shih, P.K., Prunty, J., and Mueller, R.N., "Thermostructural Concepts for Hypervelocity Vehicles," AIAA Paper 88-2295, *Proceedings of AIAA/ASME/-ASCE/AHS 29th Structures, Structural Dynamics and Materials Conference, Williamsburg, Va., April, 1988,* pp. 651–658.
2. Barthelemy, J.-F. (Editor), *Proceedings of Second NASA/Air Force Symposium on Recent Experiences in Multidisciplinary Analysis and Optimization,* Hampton, Va., Sept. 28–30, 1988, NASA CP-3031, April 1989.
3. Sobieszczanski-Sobieski, J. (Editor), *Recent Experiences in Multidisciplinary Analysis and Optimization,* NASA CP-2327, 1984.
4. Adelman, H.M., and Haftka, R.T. (Editors), *Proceedings of the Symposium on Sensitivity Analysis in Engineering,* NASA Langley Research Center, Hampton, Va., Sept. 1986, NASA CP-2457, 1987.
5. Haftka, R.T., Martinovic, Z.N., and Hallauer, W.L., "Enhanced Vibration Controllability by Minor Structural Modification," *AIAA Journal,* Vol. 23, No. 8, 1985, pp. 1260–1266.
6. Bodden, D.S. and Junkins, J.L., "Eigenvalue Optimization Algorithms for Structure/Control Design Iterations," *Journal of Guidance and Control* Vol. 8, No. 6, Nov.-Dec. 1985, pp. 679–706.
7. Khot, N.S., Eastep, F.E., and Venkayya, V.B., "Simultaneous Optimal Structural/Control Modifications to Enhance the Vibration Control of Large Flexible Structures," AIAA Paper 85-1925, *Proceedings of Guidance, Navigation and Control Conference, Snowmass, Colorado, Aug. 19–21 1985,* pp. 459–466.

8. Khot, N.S. and Grandhi, R.V., "Optimization of Structure and Control System," Second NASA/Air Force Symposium on Recent Experiences in Multidisciplinary Analysis and Optimization, Sept. 28–30, 1988, Hampton, Va.

9. Hale, A.L., Lisowski, R.J., and Dahl, W.E., "Optimal Simultaneous Structural and Control Design of Maneuvering Flexible Spacecraft," *Journal of Guidance and Control,* Vol. 8, No. 1, 1985, pp. 86–93.

10. Onoda, J. and Haftka, R.T., "An Approach to Structure/Control Optimization for Large Space Structures," *AIAA Journal,* Vol. 25, No. 8, 1987, pp. 1133–1138.

11. Balas, M.J., "Active Control of Flexible Systems," *Journal of Optimization Theory and Applications,* Vol. 25, No. 3, pp. 415–436, July, 1978.

12. Czajkowski, E. and Preumont A., "Spillover Stabilization and Decentralized Modal Control of Large Space Structures," AIAA Paper 87-0903-CP, *Proceedings of AIAA/ASME/ASCE/AHS 28th Structures, Structural Dynamics and Materials Conference and AIAA Dynamics Specialist Conference, Part 2B, Monterey, California, April, 1987,* pp. 599–609.

13. Hughes, P.C., "Space Structure Vibration Modes: How Many Exist? Which Ones Are Important?," *IEEE Control Systems Magazine,* Vol. 7, No. 1, Feb. 1987, pp. 22–28.

14. Hughes, P.C., and Skelton, R.E., "Modal Truncation for Flexible Spacecraft," *Journal of Guidance and Control,* Vol. 4, No. 3, May-June 1981, pp. 291–297.

15. Hu, A., Skelton, R.E., and Yang, T.Y., "Modeling and Control of Beam-Like Structures," *Journal of Sound and Vibration,* Vol. 117, No. 3, Sept. 1987, pp. 475–496.

16. Skelton, R.E., Hughes, P.C., and Hablani, H.B., "Order Reduction for Models of Space Structures Using Modal Cost Analysis," *Journal of Guidance and Control,* Vol. 5, No. 4, July-Aug. 1982, pp. 351–357.

17. Perry, Lt. C.O., and Venkayya, V.B., "Issues of Order Reduction in Active Control System Design," AIAA Paper 86-2138, Guidance, Navigation and Control Conference, Aug. 18–20, 1986, Williamsburg, Va.

18. Ramakrishnan, J.V., Rao, S.V., and Koual, L.R., "Reduced-Order Modeling of Flexible Structures," *Journal of Guidance and Control,* Vol. 11, No. 5, Sept.-Oct. 1988, pp. 459–464.

19. Haftka, R.T., and Yates, E.C., Jr., "Repetitive Flutter Calculations in Structural Design," *Journal of Aircraft,* Vol.13, No.7, pp. 454–461, July 1976.

20. Haftka, R.T. and Kamat, M.P., *Elements of Structural Optimization*, Martinus Nijhoff Publishers, Dordrecht, The Netherlands, 1985, pp. 172–173.

21. Leung, Y.T., "Fast Response Method for Undamped Structures," *Engineering Structures,* Vol. 5, April 1983, pp. 141-149.

22. Shore, C.P., "Reduction Method for Thermal Analysis of Complex Aerospace Structures," NASA TP 2373, Jan. 1985.

23. Cardona, A. and Idelsohn, S., "Solution of Non-Linear Thermal Transient Problems by a Reduction Method," *International Journal of Numerical Methods in Engineering,* Vol. 23, 1986, pp. 1023–1042.

24. Nour-Omid, B. and Wilson, E.L., "A New Algorithm for Heat Conduction Analysis," *Numerical Methods in Thermal Problems (Part 1),* Pineridge Press, 1985.

25. Camarda, C.J., Haftka, R.T., and Riley, M.F., "An Evaluation of Higher-Order Modal Methods for Calculating Transient Structural Response," *Computers and Structures,* Vol. 27, No. 1, 1987, pp. 89–101.

26. Borino, G. and Muscolino, G., "Mode-Superposition Methods in Dynamic Analysis of Classically and Non-Classically Damped Linear Systems," *Earthquake Engineering and Structural Dynamics,* Vol. 14, 1986, pp. 705–717.

27. Likhoded, A.I., "Convergence of the Method of Expansion in Natural Vibration Modes in Programs of Dynamic Loading," *Izv. AN SSSR. Mekhanika Tverdogo Tela,* Vol. 21, No. 1, 1986, pp. 180–188.

28. Kline, K.A., "Dynamic Analysis Using a Reduced Basis of Exact Modes and Ritz Vectors," *AIAA Journal,* Vol. 24, No. 12, 1986, pp. 2022–2029.

29. Cornwell, R.E., Craig, Jr., R.R., and Johnson, C.P., "On the Application of the Mode-Acceleration Method to Structural Engineering Problems," *Earthquake Engineering and Structural Dynamics,* Vol. 11, No. 5, Sept.-Oct. 1983, pp. 679–688.

30. Carmada, C.J., and Haftka, R.T.,"Development of Higher-Order Modal Methods for Transient Thermal and Structural Analysis," NASA TM-101548, Feb. 1989.

31. Sandridge, C.A. and Haftka, R.T., "Accuracy of Eigenvalue Derivatives From Reduced Order Structural Models," *AIAA Journal of Guidance, Control and Dynamics,* scheduled for publication April/May 1989.

32. Sandridge, C.A. and Haftka, R.T., "Effect of Modal Truncation on Derivatives of Optimal Control Performance," *Computational Mechanics 88: Theory and Applications: Proceedings of the International Conference on Computational Engineering Science, April 10–14, 1988, Atlanta, Georgia, Vol. 2,* pp. 43.v.1–43.v.4.

33. Livne, E., "Accurate Calculation of Control Augmented Structural Eigenvalue Sensitivities Using Reduced Order Models," accepted for publication, *AIAA Journal.*

34. Darnley, E.R., "The Transverse Vibration of Beams and Whirling Shafts Supported at Intermediate Points," *The London, Edinburgh and Dublin Philosophical Magazine and Journal of Science,* Ser. 6, Vol. 41, No. 241, Jan. 1921, pp. 81–96.

35. Whetstone, W.D., *EISI-EAL Engineering Analysis Language Reference Guide*, Engineering Information Systems, Incorporated, San Jose, California, 1983.

36. Reddy, J.N., *Applied Functional Analysis and Variational Methods in Engineering*, McGraw-Hill Book Company, New York, N.Y., 1986, p. 401.

37. Kwakernaak, H., and Sivan, R., *Linear Optimal Control Systems*, Wiley-Interscience, 1972.

38. Canavin, J.R., "The Control of Spacecraft Vibrations Using Multivariable Output Feedback," AIAA Paper 78–1419, AIAA/AAS Astrodynamics Conference, Palo Alto, California, Aug. 7–9, 1978.

39. Aubrun, J.–N., Ratner, M.J., and Lyons, M.G., "Structural Control for a Circular Plate," *Journal of Guidance, Control and Dynamics*, Vol. 7, No. 5, Sept.–Oct. 1984, pp. 535–545.

40. Meirovitch, L., Baruh, H., Montgomery, R.C., and Williams, J.P., "Nonlinear Natural Control of an Experimental Beam," *Journal of Guidance, Control and Dynamics*, Vol. 7, No. 4, July-Aug. 1984, pp. 437-442.

41. Anderson, B.D.O., and Moore, J.B., *Linear Optimal Control*, Prentice-Hall, Inc., 1971, pp. 50–60.

Appendix

Continuum Formulation

The eigenvalue equation for the free vibration of a Bernoulli-Euler beam is

$$\frac{d^4V}{dx^4} - \lambda^4 V = 0 \qquad (A.1)$$

where V is the transverse displacement, x is the axial coordinate, and $\lambda^4 = \rho A\omega^2/EI$ (ρ is the mass density, A is the cross-sectional area, ω is the natural frequency, and EI is the bending stiffness). The general solution of Eq. (A.1) can be written

$$V(x) = a\ \cos\lambda x + b\ \cosh\lambda x + c\ \sin\lambda x + d\ \sinh\lambda x \qquad (A.2)$$

where a, b, c, and d are constants that depend on the boundary conditions.

Following Ref. 34, we consider a five-span beam, with each span of equal length l (see Fig. 2.2). If the coordinate system of each span is at the left end of the span, then Eq. (A.2) can be written for the r^{th} span as

$$V(x) = a_r \cos\lambda x + b_r \cosh\lambda x + c_r \sin\lambda x + d_r \sinh\lambda x \qquad (A.3)$$

Since at $x = 0, V = 0$, this reduces to

$$V(x) = a_r(\cos \lambda x - \cosh \lambda x) + c_r \sin \lambda x + d_r \sinh \lambda x \qquad (A.4)$$

Further conditions that $V = 0$ at all the supports and V' and V'' are continuous at the interior supports give us the following

$$a_r(\cos \lambda l - \cosh \lambda l) + c_r \sin \lambda l + d_r \sinh \lambda l = 0 \qquad (A.5)$$

$$-a_r(\sin \lambda l + \sinh \lambda l) + c_r \cos \lambda l + d_r \cosh \lambda l = c_{r+1} + d_{r+1} \qquad (A.6)$$

$$a_r(\cos \lambda l + \cosh \lambda l) + c_r \sin \lambda l - d_r \sinh \lambda l = 2a_{r+1} \qquad (A.7)$$

Eq. (A.5) can be written for each span and Eqs. (A.6) and (A.7) can be written for each interior support. Since the moment at the left end of the beam is zero, $V''(0) = 0$; thus $a_1 = 0$. The final equation that is needed is for the moment at the right end of the beam equal to zero $[V''(l) = 0]$.

At this point, we have a 14×14 eigenvalue problem. The eigenvalues are found by solving a transcendental equation developed below. Then the constants are found by dropping one of the eigensystem equations, setting the value of one of the constants equal to one, and then solving for the rest of the constants. In this work, we dropped the last equation $[V''(l) = 0$ in last span] and assumed $c_5 = 1$.

One set of solutions corresponds to $\sin \lambda l = 0$ or

$$\lambda = \frac{n\pi}{l} \qquad (A.8)$$

For the five-span beam, this gives us the eigenvalues for every fifth mode (i.e. $\lambda_1, \lambda_6, \ldots$). The mode shapes for these frequencies are just sine functions (a_r, b_r, and c_r are zero). To find the rest of the mode shapes, Eqs. (A.5–A.7) need to be simplified.

By adding Eq. (A.5) to Eq. (A.7) and solving for c_r, and then subtracting Eq. (A.7) from Eq. (A.5) and solving for d_r, we get

$$c_r = \frac{a_{r+1} - a_r \cos \lambda l.}{\sin \lambda l} \tag{A.9}$$

$$d_r = \frac{-a_{r+1} + a_r \cosh \lambda l}{\sinh \lambda l} \tag{A.10}$$

as long as $\sin \lambda l \neq 0$. Adding c_r and d_r, we get

$$c_r + d_r = a_r \alpha - a_{r+1} \beta \tag{A.11}$$

where $\alpha = \coth \lambda l - \cot \lambda l$ and $\beta = \text{csch} \lambda l - \csc \lambda l$. Similarly, we can show that

$$c_{r+1} + d_{r+1} = a_{r+1} \alpha - a_{r+2} \beta \tag{A.12}$$

Eqs. (A.9), (A.10), and (A.12) can now be substituted into Eq. (A.6) and simplified to get

$$a_r \beta - 2a_{r+1} \alpha + a_{r+2} \beta = 0 \tag{A.13}$$

This equation can be written for each interior support, thus for our case we have four equations. As before, a_1 is zero, and since there is no sixth span, a_6 is also zero. We are left with four equations and five unknowns (a_2, a_3, a_4, a_5, and λ). If the determinant of the system is set equal to zero, we get

$$16\alpha^4 - 12\alpha^2 \beta^2 + \beta^4 = 0 \tag{A.14}$$

This equation can now be solved for the remaining eigenvalues by using a root solver and initial estimates from the finite-element model. Then the 13-equation system can be solved for the mode-shapes. Quadruple precision was needed to solve for the higher frequency mode shapes because the hyperbolic functions made the

system singular. The frequencies found from Eq. (A.14) fill in the gaps between those given in Eq. (A.8).

Once all the desired frequencies and mode shapes are calculated, generalized system matrices can be generated in order to calculate damping ratios and their derivatives. This is done by assuming that the damped modes can be approximated by a linear combination of the natural modes above. Using N modes, the damped mode V_r is obtained by solving the eigenvalue problem Eq. (2.14), where $\hat{M}$ and $\hat{K}$ are $N \times N$ diagonal matrices with the generalized masses and stiffnesses on the diagonals. The generalized mass (m_i) and generalized stiffness (k_i) for the i^{th} mode ψ_i are calculated as follows:

$$m_i = \rho A \int_0^l \psi_i^2 dx \tag{A.15}$$

$$k_i = EI \int_0^l (\psi_i'')^2 dx \tag{A.16}$$

Since the integrands are products of trigonometric functions, the integrals can be calculated analytically. The damping matrix for the system is a full matrix calculated as follows:

$$c_{ij} = c_1 \psi_i(x_{c_1}) \psi_j(x_{c_1}) + c_2 \psi_i'(x_{c_2}) \psi_j'(x_{c_2}) \tag{A.17}$$

where x_{c_1} and x_{c_2} are the location of the controllers. The derivative of the damping ratios were calculated using central finite differences as

$$\frac{\partial \varsigma_r}{\partial m} \cong \frac{\varsigma_r(\Delta M) - \varsigma_r(-\Delta M)}{2\Delta m} \tag{A.18}$$

where ΔM is a full $N \times N$ matrix corresponding to the added mass Δm in generalized coordinates. The elements of ΔM are

$$\Delta M_{ij} = \Delta m \psi_i(x_{\Delta m}) \psi_j(x_{\Delta m}) \tag{A.19}$$

where $x_{\Delta m}$ is the location of the added mass.

The vita has been removed from the scanned document